Strongly interacting two-component coupled Bose gas in optical lattices

Sagarika Basak [*] and Han Pu [†]

Department of Physics and Astronomy & Rice Center for Quantum Materials, Rice University, Houston, Texas 77251, USA

Two-component coupled Bose gas in a 1D optical lattice is examined. In addition to the postulated Mott insulator and superfluid phases, multiple bosonic components manifest spin degrees of freedom. Coupling of the components in the Bose gas leads to substantial changes in the previously observed spin phases, giving rise to a new effective spin Hamiltonian and unraveling remarkable spin correlations. The system in the absence of coupling exhibits ferromagnetic and nonferromagnetic spin phases for on-site intracomponent interaction stronger than intercomponent interaction. Upon introduction of coupling, the phase transition switches from first to second order. For comparable on-site inter- and intracomponent interactions, with coupling, instead of one, two spin phases emerge with a second-order phase transition. Exact diagonalization and variational Monte Carlo with stochastic minimization on the entangled-plaquette state bestow a unique and enhanced perspective on the system beyond the scope of a mean-field treatment.

I. INTRODUCTION

Ultracold gases provide an unparalleled platform to explore physics found in atomic or molecular gases, offering a manifold of prospects to simulate and examine canonical models of strongly correlated electrons in condensed matter systems [1,2], owing to them being clean, versatile, and highly controllable. Observation of the superfluid to Mott insulator transition [3] and theoretical and experimental demonstration of exotic quantum phase transitions [4] in cold-atomic setups have paved the way toward studying many-body physics [1,2,5–7], in association with strong correlations [3,8], and relating to the emergence of collective and thermodynamic behavior [5,9]. Experimental demonstrations—of cold atoms in lattices via weak trapping potential superimposed onto optical lattices [6], achievement of low temperature relevant for spin orders [1,10–12] necessary for superexchange couplings resulting in effective nearest-neighbor spin-spin interaction demonstrated in an array of double wells [13] via a combination of evaporative and adiabatic cooling [14–21], and simulating magnetic fields via artificial gauge potential [22,23]—provide immense relevance to this field. Quantum magnetism, a most fascinating area of research in condensed matter physics, can be reproduced using cold atoms with tunable geometry and parameters: for instance, experimental study of itinerant magnetism in ultracold Fermi systems with repulsive interactions [24], classical magnetism in triangular lattices [25] with fast oscillations of the optical lattice enabling tuning the sign of nearest-neighbor tunneling [26], bosons with strong interactions in a tilted lattice at commensurate fillings for the study of the Ising model and quantum phase transition [27,28], and possible realization of quantum dimer models [27,29].

The Bose-Hubbard Hamiltonian describing the dynamics of bosonic atoms is a quintessential model to probe strongly correlated many-body quantum systems [5,30,31] and simulate lattice spin models [1,2,31–39] such as the quadratic-biquadratic spin model [40], or antiferromagnetic spin chains [27] and a spin-1 model exhibiting the Haldane (gapped) insulator phase [41–45]. Interesting extensions of the Bose-Hubbard model, such as inclusion of next-nearest-neighbor tunneling or long-range interactions [46–51], spinor bosons with multiple internal degrees of freedom [52,53], and addition of nonlinear coupling between the components [54–59], display remarkably rich phase diagrams [47,56–59]. A two-component Bose-Hubbard model in the Mott phase reveals pseudospins effectively coupled by the Heisenberg exchange [38] imitating a spin-$\frac{1}{2}$ Hamiltonian ideal for the study of quantum magnetism [38,60,61], displays a spin-Mott phase in the spin-1 Hamiltonian [11,38,39,60,62,63], and in the presence of strong repulsions presents a finite-temperature phase structure with the possibility of checkerboard long-range order, supercounterflow, superfluidity, and phase separation [64]. Realization of controllable Bose-Bose mixtures [65] makes way for the experimental reproduction of spin Hamiltonians, with detection and study of magnetic phases such as antiferromagnetic Néel and *xy* ferromagnetic phases.

The physics of coherent coupling in ultracold gases is consequential for quantum information processing and simulation [31,37], supported by the demonstration of strong coupling between bosonic Mott insulators and light [66,67] and the recent work in cold atoms proposing the realization and manipulation of new quantum states [68–75] and high-precision quantum limited measurements [76]. In the two-component Bose gas, introducing coupling reveals fascinating physics: for instance, the phase separation in the weak-interaction limit [77] changing dramatically [78–89], modifying the Mott insulator–superfluid transition [90], and altering entanglement properties [91]. With the introduction of nonlinear coupling in many-body systems, stable collective

---

[*]basak.sagarika@rice.edu

[†]hpu@rice.edu

modes appear, thus paving the way for robust control [92,93], with their localization properties and robustness against perturbations demonstrated in a tilted Bose-Hubbard model [94].

Here, we study Bose gas with two components trapped in a one-dimensional (1D) optical lattice, realizing a two-component Bose-Hubbard model. The presence of multiple bosonic components manifests spin degrees of freedom in addition to the Mott insulator and superfluid phases [38,60]. The coupling of the two components on the nearest-neighbor sites with strong on-site interactions presents unconventional effective ordering generating unprecedented spin behavior. The formation of a new site-dependent nonferromagnetic spin phase occurs owing to this coupling. The choice of spin alignment along z in this phase can be tuned using hopping parameters. The signature of this unique phase appears as an oscillation in spatial z-x spin correlation between spins, whereas it remains constant (≈ 0) in a conventional antiferromagnetic spin phase. In addition to the creation of the unconventional nonferromagnetic spin phase, the coupling also significantly alters the phase space. When the intra-component interaction is stronger than the intercomponent interaction, the introduced coupling switches the phase transition between ferromagnetic and nonferromagnetic spin phases from first order to second order, with the transition width dependent on coupling. When these interactions are comparable, two spin phases (ferromagnetic and nonferromagnetic) are displayed instead of one (ferromagnetic) with a second-order phase transition, when coupling is introduced. This study provides a spin-independent implementation of the optical lattice for trapping the two-component Bose gas with no additional tuning of on-site interaction strengths and instead leveraging coupling as a parameter to switch between the different spin phases. Multiple perspectives—obtained from methods based on mean-field approximation, exact diagonalization, and entangled-plaquette states (EPS)—enhance the understanding of this system, capturing correlations beyond the scope of a mean-field treatment. The physics of a filling factor greater than unity where the novel spin correlations persist and the consideration of complex intracomponent tunneling and intercomponent coupling are discussed.

This paper is sectioned as follows: Section II describes the coupled two-component Bose-Hubbard model and its realization. Section III details the mapped spin-$\frac{1}{2}$ model. Section IV presents the different numerical methods considered in the study. Section V is the multiperspective study of the spin phases. Section VI goes on to discuss complex intracomponent tunneling and intercomponent coupling, as well as the physics of occupancy greater than unity. Finally, Sec. VII summarizes the results and discusses their implications and future avenues.

II. THE MODEL

We consider a 1D system comprising two kinds of bosons trapped in a spin-independent optical lattice as shown in Fig. 1. The two components termed, a and b, can be envisioned as two internal levels of an atom. We assume low temperature and the optical lattice to be deep enough for the atoms to be confined to the lowest Bloch band describing a two-component Bose-Hubbard model [39,95]. The optical
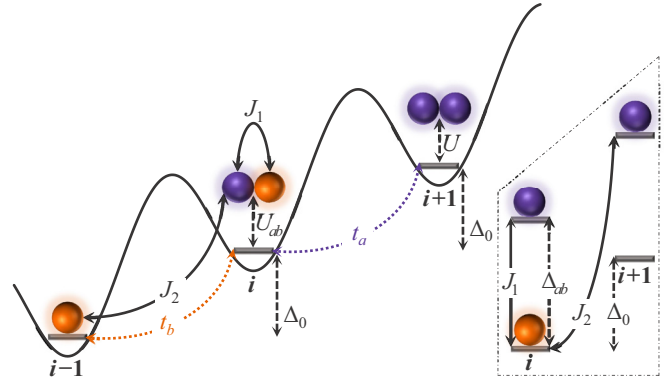

FIG. 1. Two-component Bose-Hubbard model with on-site inter- (U_{ab}) and intra- (U) component interaction ($U \gg U_{ab}$ and $U \sim U_{ab}$) with nearest-neighbor tunneling coefficients t_a and t_b. The optical lattice is tilted via external inhomogeneous static electric or magnetic field. Inset: To the system is introduced laser-assisted intercomponent coupling: J_1 (same site) and J_2 (nearest neighbor). The two components are visualized as two levels of an atom.

lattice is tilted, creating an energy offset between the nearest-neighbor sites as shown in Fig. 1, with the assumption that the potential applied to create this tilt is a perturbation. This tilt can be introduced using a magnetic field gradient [96,97]. The tilting of the lattice prevents the natural hopping between components a (or b) that is obtained via light-assisted tunneling: the resonant two-photon Raman transition [96]. We introduce to this system intercomponent coupling, also obtained by a resonant two-photon Raman transition between two internal states as shown in Fig. 1 (inset). The resulting system is governed by the following Hamiltonian:

$$
\begin{aligned}
H = & \sum_i (-t_a a_i^\dagger a_{i+1} - t_b b_i^\dagger b_{i+1} + \text{H.c.}) \\
& + \sum_{k=a,b;i} \frac{U}{2} n_{ki}(n_{ki} - 1) + \sum_i U_{ab} n_{ai} n_{bi} \\
& - \sum_i J_1 (a_i^\dagger b_i + b_i^\dagger a_i) - \sum_i J_2 (b_i^\dagger a_{i+1} + a_{i+1}^\dagger b_i), \quad (1)
\end{aligned}
$$

where a_i and b_i are the bosonic annihilation operators for components a and b at site i, respectively. t_k is the component-dependent tunneling parameter. U is the intra- and U_{ab} the intercomponent on-site interaction strength. Two kinds of intercomponent couplings are present: J_1 and J_2 representing the same-site and nearest-neighbor coupling, respectively. The energy offset between nearest-neighbor sites of the optical lattice (Fig. 1) differentiates the couplings, where J_2 defines the intercomponent coupling between b at site i and a at site $i + 1$. The presence of this offset also allows for tuning of J_1 and J_2 independently (Fig. 1, inset). In the deep Mott limit ($U, U_{ab} \gg t_k, J_1, J_2$), with the average number of particles per site being fixed due to the high energy cost of bosons hopping between sites, this model can be mapped to an effective spin system. In the following sections, we study the system in the deep Mott limit, specifically for the case of one particle per site that is mapped to spin-$\frac{1}{2}$, where a: $\uparrow$ and b: $\downarrow$.

III. EFFECTIVE SPIN HAMILTONIAN

Strong on-site interactions divide the Hilbert space into low- and high-energy subspaces, which are coupled by the coupling and tunneling terms as shown in Fig. 2. A particle hopping from one site to another increases the occupancy, thus going from a low- to high-energy subspace, and thus incurring high energy cost in the process, whereas two particles exchanging positions preserve the occupancy and hence do not require a high energy cost. To study the relevant physics, the effective low-energy subspace is obtained by decoupling the existing subspaces, removing any first-order hopping that increases the occupancy and retaining the second-order virtual hopping terms that preserve the occupancy.

The two-component Bose-Hubbard model is mapped to the following effective spin (low-energy) Hamiltonian via canonical transformation and followed by a perturbative expansion up to second order (for details, see Appendix A):

$$H_{\text{eff}} = \sum_i \left[-J_\perp \left(\sigma_i^x \sigma_{i+1}^x + \sigma_i^y \sigma_{i+1}^y \right) - J_z \sigma_i^z \sigma_{i+1}^z - h_z \left(\sigma_i^z \right) \right.$$
$$\left. - (h_x + J_1) \sigma_i^x + J_{zx} \sigma_i^z \sigma_{i+1}^x - J_{xz} \sigma_i^x \sigma_{i+1}^z \right], \quad (2)$$

where
$$J_\perp = \frac{t_a t_b}{U_{ab}},$$
$$J_z = \left(t_a^2 + t_b^2 - J_2^2 \right) \left(\frac{1}{U} - \frac{1}{2U_{ab}} \right),$$
$$h_z = \frac{2 \left(t_a^2 - t_b^2 \right)}{U},$$
$$h_x = J_2 (t_a + t_b) \left(\frac{1}{U_{ab}} + \frac{1}{U} \right),$$
$$J_{zx} = \frac{J_2 t_b}{U},$$
$$J_{xz} = \frac{J_2 t_a}{U}.$$

$J_\perp$ and J_z provide the xy and z ordering, respectively. The xy ordering is always ferromagnetic in nature, while the z ordering can be tuned from ferromagnetic to antiferromagnetic by varying the parameters t_a, t_b, and J_2. The terms h_z and h_x, J_1 act as fictitious magnetic fields along z and x, respectively, transforming the system to a spin-polarized state. Unconventional ordering terms, J_{zx} and J_{xz}, arise due to the directional nearest-neighbor intercomponent coupling. They tend to align the spins along x on one site and along z on the nearest-neighbor sites, providing a straightforward implementation for site-dependent spin alignment. That the tunnelings and coupling are light assisted and the on-site interactions controllable via external magnetic field (Feshbach resonance) allows for the effective parameters to be tuned over a rather large range. Presently only J_2 is considered as J_1, with no energy cost in same-site coupling, trivially leads the system to an x ferromagnetic phase. With the introduction of nearest-neighbor intercomponent coupling, we see new ordering terms h_x, J_{xz}, and J_{zx}; their significance is understood
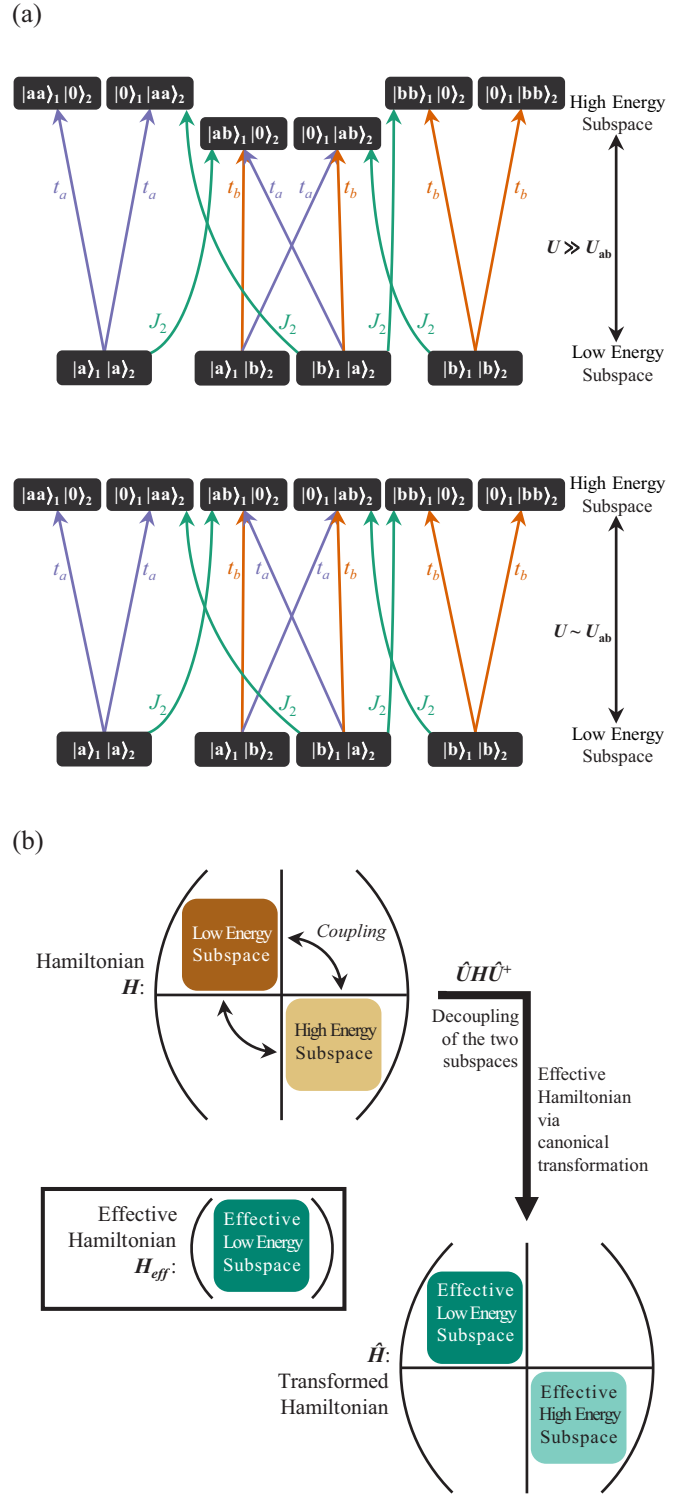

FIG. 2. Schematic of the effective spin Hamiltonian. (a) The low- and high-energy subspaces for a two-site system, roughly separated by the on-site interaction strength and coupled by the intercomponent coupling and intracomponent tunneling coefficients. (b) The Hamiltonian with low- and high-energy subspaces forming the diagonal with the off-diagonal coupling and tunneling coefficients coupling the two subspaces and the effective decoupling of the two subspaces to obtain the effective low-energy spin Hamiltonian.

by studying the system behavior dictated by parameters t_a, t_b, and J_2.

IV. NUMERICAL METHODS

Three different methods are utilized in our study: (a) mean-field approximation, (b) exact diagonalization for small system size ($N < 14$), and (c) variational Monte Carlo with stochastic minimization (VMC-SM) on entangled-plaquette states (EPSs) for large system size ($N \geqslant 14$).

Mean-field approximation is the simplest approach pursued. Here, each site is treated independently of the others, making it computationally efficient. Additionally, it is unaffected by the system size. To illustrate the spin phases within mean field, we designate each alternating site to subspace A and its nearest-neighbor sites to subspace B. The following variational ansatz is considered:

$$|\Psi\rangle = \prod_{i\in A}[\cos(\theta_A)\,|a\rangle_i + \sin(\theta_A)\,|b\rangle_i]$$
$$\times \prod_{i+1\in B}[\cos(\theta_B)\,|a\rangle_{i+1} + \sin(\theta_B)\,|b\rangle_{i+1}]. \quad (3)$$

Within the mean-field approximation, the spin order along x and z is computed using Pauli matrices:

$$\langle\sigma^x_{i\vee i+1}\rangle = \sin 2\theta_{A\vee B}, \quad \langle\sigma^z_{i\vee i+1}\rangle = \cos 2\theta_{A\vee B}. \quad (4)$$

The simplicity of the mean-field approximation, in treating each site independently of others, may not accurately reflect the system behavior due to the presence of spin exchanges in the effective spin Hamiltonian correlating nearest-neighbor sites. This could dilute the effect of the unconventional correlations by their being beyond the scope of the mean-field treatment.

Exact diagonalization (ED) provides the most accurate description of the system. Devoid of any approximations, it is the most successful in capturing the effect of the unconventional correlations. Additionally it provides direct comparisons to $N = 2$ (see Appendix B), where the effective spin Hamiltonian [Eq. (2)] is benchmarked against the original Hamiltonian [Eq. (1)] and validated. Although the exact diagonalization does provide a better insight into the system, owing to its large computational expense, this is limited to smaller system sizes $N < 14$, where the effect of small system size can be observed. For the thermodynamic limit, a need arises for a numerical method that captures correlations better than the mean-field treatment but with lesser computational expense than exact diagonalization.

Entangled-plaquette states (EPSs) form a class of tensor network states, where the lattice is divided into plaquettes, and the wave function of the system is given by the product of the plaquette wave functions, which are scalar in nature [98]. This goes beyond the mean field, by considering overlapping or entangled plaquettes, and is more computationally efficient than exact diagonalization as the number of steps to obtain the system ground state undergo a low-order polynomial increase with system size. It allows for large system sizes while retaining most of the effects of the correlations. In our ansatz with overlapping plaquettes (P), each consisting of four sites, coefficients ($C_P^{\mathbf{n}_P}$; correlator elements) are assigned for all 2^4
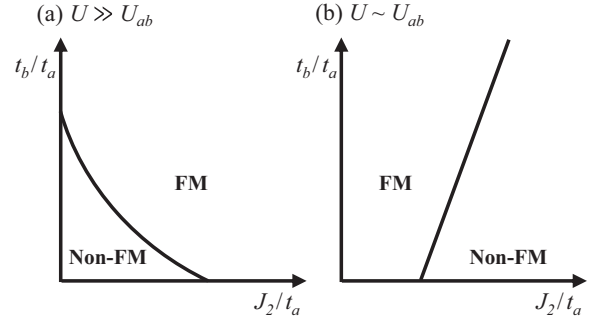

FIG. 3. Schematic of spin phases hypothesized to emerge in the presence of intercomponent coupling (J_2). The phases are shown in the deep Mott regime, (a) $U \gg U_{ab}$ and (b) $U \sim U_{ab}$, and presented as a function of scaled intracomponent tunneling $\frac{t_b}{t_a}$ and intercomponent coupling $\frac{J_2}{t_a}$. The FM phase demonstrates typical behavior, with spin along x or z. The non-FM phase demonstrates a typical zAFM, and an unconventional non-FM phase. A key feature of the unconventional phase: a spin along z on one site correlated with a spin along x on another site.

possible configurations in each plaquette. The amplitude for each spin configuration in the state is given as a product of these correlator elements [99]. Variational Monte Carlo (VMC) with stochastic minimization (SM) [98] is used to obtain the optimized plaquette wave functions that minimize the energy and best describe the ground state.

Concurrent employment of all three methods in our analysis helps in validating each method and identifying areas where they fail. It also facilitates an accurate interpretation of the results that best reflect the system behavior, with minimal effect of the system size and the approximations made in the mean-field treatment.

V. SPIN PHASES

Previous work studying the two-component Bose-Hubbard model in the absence of intercomponent coupling shows two spin phases: xy ferromagnetic (FM; $t_a \sim t_b$) and z antiferromagnetic (AFM; $t_{a\vee b} \gg t_{b\vee a}$) with a first-order phase transition [39]. This is only seen in the on-site interaction limit $U \gg U_{ab}$. In the other limit $U \sim U_{ab}$, only one spin phase—zFM—exists. Motivated by these, we explore the spin phase space in the presence of coupling for strong on-site intra- and intercomponent interaction in the limits $U \gg U_{ab}$ and $U \sim U_{ab}$. A schematic of the spin phases in the presence of coupling is shown in Fig. 3, surmised from the effective Hamiltonian. For $U \gg U_{ab}$, when $t_{a\vee b} \gg t_{b\vee a}$, introducing coupling ($J_2$) evolves the zAFM in the non-FM phase to an unconventional non-FM phase arising due to J_{xz} and J_{zx}. Further increase in J_2 transitions this to xFM in the FM phase due to h_x, eventually evolving to a zFM phase due to J_z. When $t_a \sim t_b$ and $J_2 = 0$, an xyFM phase is displayed. With coupling, this becomes an xFM due to h_x. For $U \sim U_{ab}$, with increasing J_2, the system evolves from biased zFM to xFM in the FM phase, transitioning to the unconventional non-FM and evolving to a zAFM in the non-FM phase.

We now introduce coupling to the system and study the spin phases that arise by evaluating the spin order parameters. The site-dependent nature of the unconventional phase
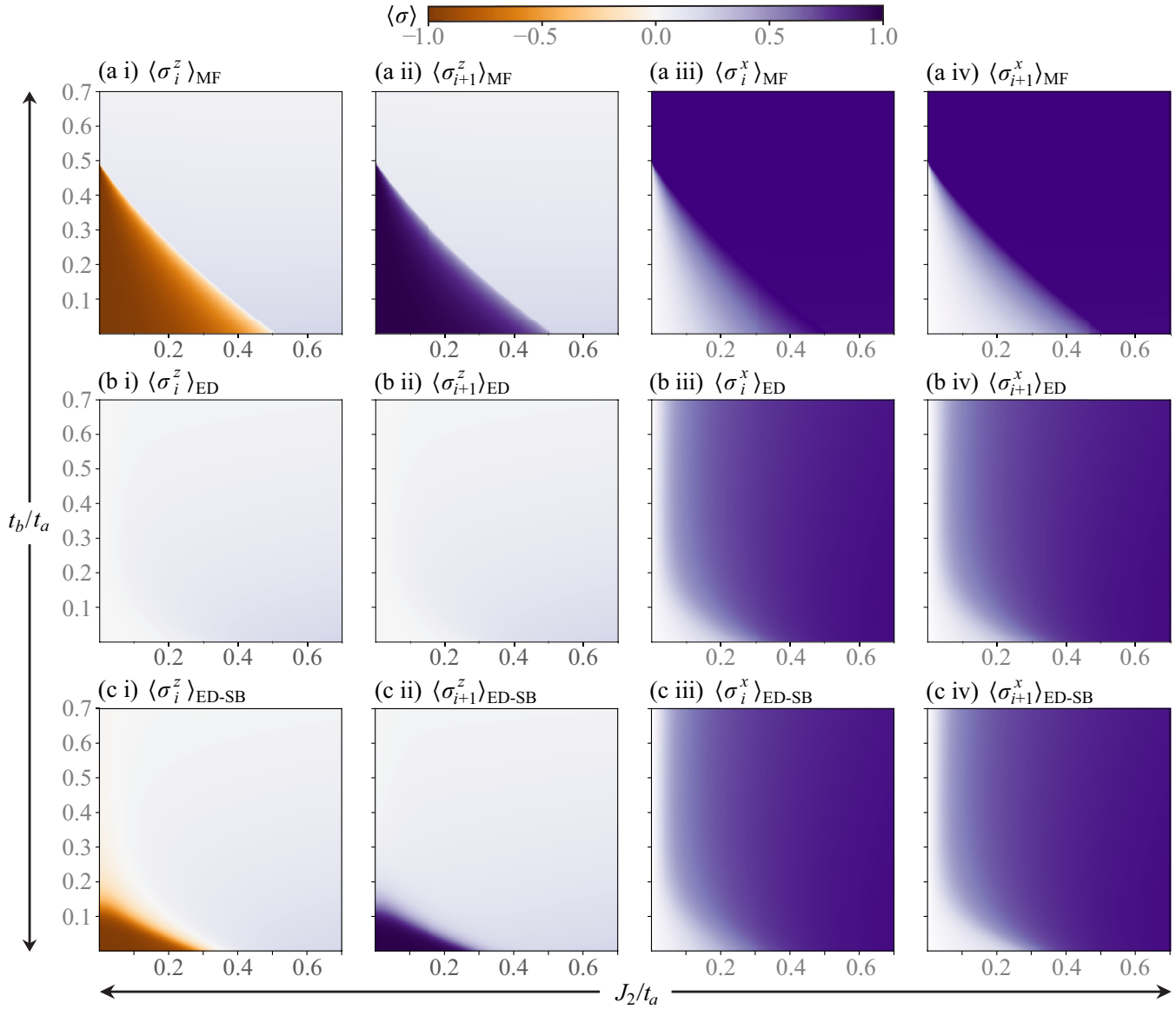
FIG. 4. Spin order parameters, describing the spin behavior along [(i) and (ii)] z and [(iii) and (iv)] x at site i in subspace A and $i + 1$ in B. The orders evaluated via (a) mean-field approximation, (b) exact diagonalization for $N = 8$, and (c) ED with the symmetry-breaking term ($\delta h_z = 4 \times 10^{-4} t_a$) for $N = 8$ are shown as a function of scaled tunneling ($\frac{t_b}{t_a}$) and coupling ($\frac{J_2}{t_a}$), in the deep Mott regime ($\frac{U}{U_{ab}} = 10$, $\frac{U_{ab}}{t_a} = 20$).

emerging due to the unique correlations is confirmed with the examination of the correlation between spins at two different sites. The spin orders along z and x on the nearest-neighbor sites depict the existence of two phases in our system: (1) spins aligning along the same direction (FM) at large tunneling ($\frac{t_b}{t_a}$) or coupling ($\frac{J_2}{t_a}$) for $U \gg U_{ab}$ (or at tunneling $\geqslant$ coupling for $U \sim U_{ab}$) and (2) spins aligning along different directions (non-FM) otherwise, as seen in Fig. 4. Figure 4, panels (a i) and (a ii) representing the spin behavior along z in the mean-field limit, displays a superposition of the quaside-generate states (reflecting either of the two degenerate spin configurations—$\uparrow_j \downarrow_{j+1}$ or $\downarrow_j \uparrow_{j+1}$—on the nearest-neighbor sites) in the non-FM phase, while Fig. 4, panels (b i) and (b ii), obtained via exact diagonalization with periodic boundary conditions, shows the true ground state (reflecting a superposition of the two spin configurations). The ground

state obtained via exact diagonalization is symmetric, whereas the state obtained in mean-field treatment has a broken symmetry.

To demonstrate correspondence of the mean-field treatment with exact diagonalization, a weak symmetry breaking term $(-\delta h_z \sum_{i \in (2\mathbb{N}+1)} \sigma_i^z)$ is introduced to the effective Hamiltonian and studied via exact diagonalization (ED-SB). The symmetry seen in ED [Fig. 4(b)] is then explicitly broken [Fig. 4(c)]. This enforces the selection of one of the two degenerate spin configurations. Spin orders—$\langle \sigma_i^{z \vee x} \rangle_{\text{ED-SB}}$—for this symmetry-broken system [Fig. 4, panels (c i) and (c ii)] present similar behavior to that in the mean-field treatment [Fig. 4, panels (a i) and (a ii)]. This concordance between ED-SB and the mean-field treatment confirms the latter results in spontaneous symmetry breaking forming a symmetry-broken ground state.
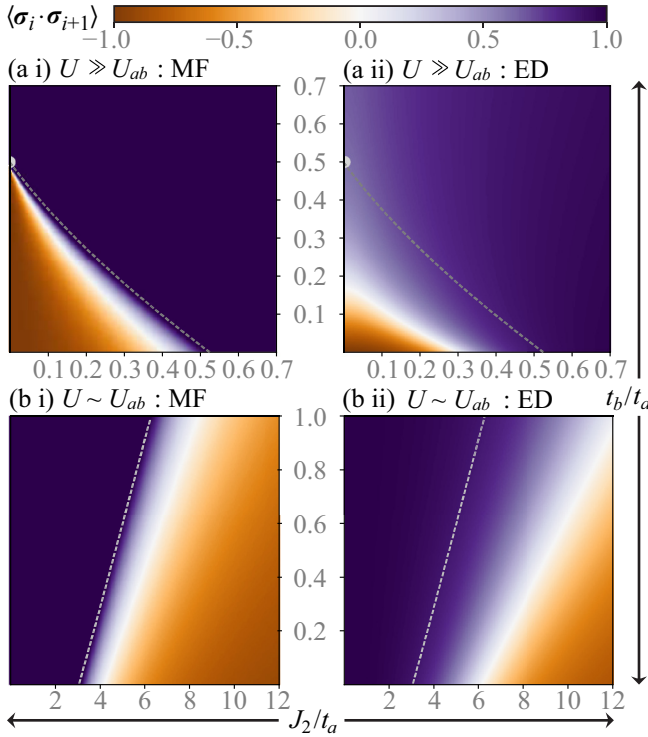
FIG. 5. Spin correlation describing the spin relationship between the nearest-neighbor sites at (a) $\frac{U}{U_{ab}} = 10$ and (b) $\frac{U}{U_{ab}} = 1.2$ evaluated via (i) mean-field approximation and (ii) exact diagonalization for $N = 8$. The correlation is shown as a function of scaled tunneling ($\frac{t_b}{t_a}$) and coupling ($\frac{J_2}{t_a}$), in the deep Mott regime ($\frac{U_{ab}}{t_a} = 20$). The dashed curve denotes the mean-field critical values ($\frac{t_b}{t_a}$)^C from Eq. (5).

In the limit $U \gg U_{ab}$ (as well as $U \sim U_{ab}$; see Fig. 5), the system in the presence of coupling shows a second-order phase transition that appears as a discontinuity in the spin orders. The critical expression for tunneling $\frac{t_b}{t_a}$ as a function of coupling $\frac{J_2}{t_a}$, and interactions U, U_{ab} describing the phase boundary, can be obtained analytically within the mean-field treatment (see Appendix C):

$$\left(\frac{t_b}{t_a}\right)^C_{U \gg U_{ab}} = -A - B \quad \text{and} \quad \left(\frac{t_b}{t_a}\right)^C_{U \sim U_{ab}} = -A + B, \quad (5)$$

where

$$A = \left(\frac{\frac{J_2}{t_a}(U + U_{ab}) + 2U}{2(2U_{ab} - U)}\right) \quad \text{and}$$

$$B = \sqrt{\left(\frac{\frac{J_2}{t_a}(U + U_{ab}) + 2U}{2(2U_{ab} - U)}\right)^2 - \left(1 - \frac{J_2^2}{t_a^2} + \frac{\frac{J_2}{t_a}(U + U_{ab})}{2U_{ab} - U}\right)}.$$

The spin correlation ($\langle \boldsymbol{\sigma}_i \cdot \boldsymbol{\sigma}_{i+1} \rangle$) between the nearest-neighbor sites is presented in Fig. 5, which demonstrates the non-FM (<1) phase and the FM ($=1$) phase, with the approximate critical tunneling coefficient $\frac{t_b}{t_a}$ describing the phase boundary. For $U \gg U_{ab}$, a first-order transition occurs along the vertical axis (i.e., $J_2 = 0$). This transitions shifts to second order as the coupling is introduced, with the transition width increasing with coupling. The spin correlation obtained via

exact diagonalization confirms the existence of the two spin phases. The difference between the mean-field approximation and exact diagonalization is expected due to the treatment of all sites independently of each other in the mean-field treatment. Additionally, the exact diagonalization is restricted to smaller system sizes.

$U \gg U_{ab}$. In the absence of coupling, dependent on the competing energy parameters J_z and $J_\perp$, the system displays zAFM for $J_z \gtrsim J_\perp$ and xyFM for $J_z < J_\perp$ [39]. These phases appear due to the high energy cost of the intermediate state $|aa\rangle_j$ or $|bb\rangle_j$ when compared to $|ab\rangle_j$. This results in a high tunneling probability for states $|a\rangle_j |b\rangle_{j+1}$ or $|b\rangle_j |a\rangle_{j+1}$.

Introducing coupling to this system, the conventional zAFM spin phase evolves to the unconventional non-FM phase as depicted in Fig. 4. The unconventional phase demonstrates a spin along z on one site correlated to a spin along x on another site. This results in a stronger z order at one site and x order at the nearest-neighbor sites in the mean-field limit forming a site-dependent spin phase. Spin orientation along z in this phase depends on the intracomponent tunneling, with up spin at $\frac{t_b}{t_a} < 1$ and down spin at $\frac{t_b}{t_a} > 1$, and thus is an intracomponent tunneling dependent spin phase. The coupling in the system allows component b on some site j to tunnel to a on site $j + 1$ or vice versa. This and the system preference for the high-energy intermediate state $|ab\rangle$ allows the nearest-neighbor sites to have the same component ($|a\rangle_j |a\rangle_{j+1}$ or $|b\rangle_j |b\rangle_{j+1}$) and delocalize. These allowed states along with the preferred configuration in the absence of coupling form the unconventional phase; in the Hamiltonian: emergent due to correlations induced by the J_{xz} and J_{zx} terms and preferentially chosen by the effective ordering h_x and h_z.

The system transitions to the FM phase forming an xFM phase upon further increase of the coupling or tunneling. At large tunneling and in the absence of coupling, an xyFM phase forms as shown in the previous work [39]. However, this preference changes with the introduction of coupling as seen in Fig. 4, forming an xFM phase, due to the strong h_x ordering.

$U \sim U_{ab}$. Similar spin phases to those in $U \gg U_{ab}$ are observed but at different regions of the phase space. In this limit, all the high-energy intermediate states have equivalent energy cost associated with them unlike the previous interaction limit. In a strong-coupling limit ($\frac{J_2}{t_a} \gg \frac{t_a}{t_b}, 1$), the conventional zAFM spin phase emerges due to the strong effective ordering along z: J_z as seen in Fig. 5, panels (b i) and (b ii). With no significant intraparticle tunneling, only the component b at some site j is allowed to tunnel to a at site $j + 1$ (or vice versa). The coupling allows for the highest tunneling probability of the configuration $|a\rangle_j |b\rangle_{j+1}$ or $|b\rangle_j |a\rangle_{j+1}$. This results in the formation of the observed zAFM phase. Allowing one component to tunnel by a small increase in intracomponent tunneling $t_{a \vee b}$ ($J_2 > t_{a \vee b} > t_{b \vee a}$) forms the unconventional non-FM phase.

When one component's intracomponent tunneling is as strong as the coupling ($J_2 \sim t_{a \vee b} \gg t_{b \vee a}$), the FM phase exists as seen in Fig. 5, panels (b i) and (b ii). It is expected that when a component is allowed to tunnel, it would be preferred on all sites. This leads to the spin-up zFM for $t_a \gg t_b$ and spin-down zFM for $t_b \gg t_a$. However, this preference changes with strong coupling, forming an xFM phase due to h_x ordering. With both components being allowed to hop, the
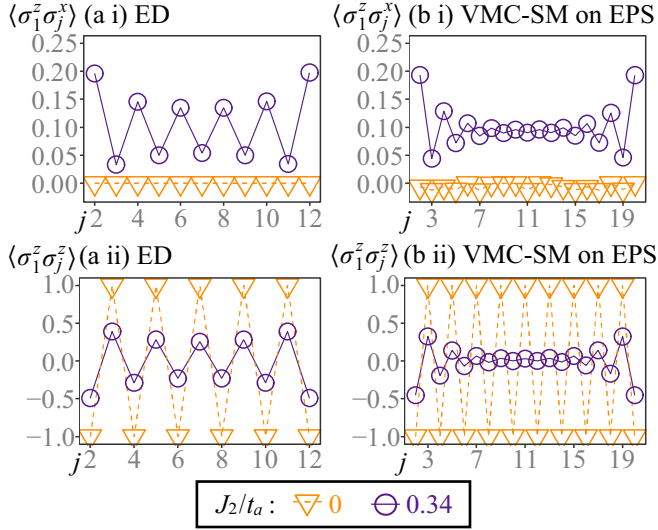
FIG. 6. Spin correlations describing the spin relationship between site 1 and some site j along (i) z-x and (ii) z, for (a) $N = 12$ via exact diagonalization and (b) $N = 20$ via VMC-SM on EPS. The correlations are shown as a function of site j at $\frac{J_2}{t_a} = 0.34$, $\frac{t_b}{t_a} = 0.0$ and $\frac{J_2}{t_a} \approx 0.0$, $\frac{t_b}{t_a} = 0.0$ in the deep Mott regime ($\frac{U_{ab}}{t_a} = 20$, $\frac{U}{U_{ab}} = 10$).

system exists in an equal superposition of components. The spin correlations obtained via exact diagonalization are comparable to the mean-field treatment for correlations along z and x.

Unconventional non-FM. The spin orders in exact diagonalization do not display (Fig. 4) the conventional zAFM and the unconventional non-FM phase as seen in the mean-field treatment. Exact diagonalization shows a superposition of all possible degenerate configurations; hence the spin orders along z show no order in the non-FM region, and the phase can only be identified by the strength of the x order, while the mean-field treatment shows one of the degenerate configurations as a result of spontaneous symmetry breaking. To demonstrate the existence of the unconventional non-FM phase, the spatial spin correlations are studied along z-x and z via exact diagonalization ($N = 12$) and VMC-SM on EPS ($N = 20$). Figure 6(a) presents the evidence of the unconventional site-dependent non-FM phase distinct from the conventional (zAFM) spin phase. Illustrated here are the spin correlations between site 1 and some site j along z-x and z obtained via exact diagonalization for system size $N = 12$ at $U \gg U_{ab}$. The unique correlations (J_{xz} and J_{zx} terms in the Hamiltonian) manifests as the observed site-dependent oscillations in the spin correlation along z-x. In the conventional regime, however, the z-x spin correlation remains constant as a function of site j ($\approx$0). The oscillation in the spatial correlation acts as a signature of this unconventional non-FM phase, and evidence of its existence in exact diagonalization. Similar oscillations appear for $U \sim U_{ab}$ albeit in a large-coupling regime ($\frac{J_2}{t_a} \approx 5$). Figure 6(b) shows the spin correlations extended to a larger system size of $N = 20$ to observe the decay in oscillation of the correlation, expected in 1D owing to the lack of true long-range order.

VI. EXTENSION

In this section we discuss the effect of complex tunneling and coupling coefficients on the spin phases, and extend our study to comment on the effective spin system at occupancy greater than unity.

Complex coefficients. Complex phases are associated with the nearest-neighbor intracomponent tunnelings t_a and t_b and the intercomponent coupling J_2 resulting in new hopping parameters: $t_a = |t_a|e^{i\theta_a}$, $t_b = |t_b|e^{i\theta_b}$, and $J_2 = |J_2|e^{i\theta_J}$. The Hamiltonian for the resulting system

$$
\begin{aligned}
H = & -\sum_i (|t_a|e^{i\theta_a} a_i^\dagger a_{i+1} + |t_b|e^{i\theta_b} b_i^\dagger b_{i+1} \\
& + |J_2|e^{i\theta_J} b_i^\dagger a_{i+1} + \text{H.c.}) \\
& + \sum_{k=a,b;i} \frac{U_k}{2} n_{ki}(n_{ki} - 1) + \sum_i U_{ab} n_{ai} n_{bi}. \quad (6)
\end{aligned}
$$

The mapped effective spin Hamiltonian in the presence of complex coefficients

$$
\begin{aligned}
H_{\text{eff}} = & -J_z \sum_i \sigma_i^z \sigma_{i+1}^z - h_z \sum_i \sigma_i^z \\
& - J_p \sum_i \big[\cos(\theta_a - \theta_b)\big(\sigma_i^x \sigma_{i+1}^x + \sigma_i^y \sigma_{i+1}^y\big) \\
& + \sin(\theta_a - \theta_b)\big(\sigma_i^x \sigma_{i+1}^y - \sigma_i^y \sigma_{i+1}^x\big)\big] \\
& - h_x \sum_i \big\{ [t_a \cos(\theta_a - \theta_J) + t_b \cos(\theta_b - \theta_J)]\sigma_i^x \\
& - [t_a \sin(\theta_a - \theta_J) + t_b \sin(\theta_b - \theta_J)]\sigma_i^y \big\} \\
& - J_{xz} \sum_i \cos(\theta_a - \theta_J)\sigma_i^x \sigma_{i+1}^z - \sin(\theta_a - \theta_J)\sigma_i^y \sigma_{i+1}^z \\
& + J_{zx} \sum_i \cos(\theta_b - \theta_J)\sigma_i^z \sigma_{i+1}^x - \sin(\theta_b - \theta_J)\sigma_i^z \sigma_{i+1}^y.
\end{aligned}
$$
$$(7)$$

The ferromagnetic ordering (J_p) of nearest-neighbor sites along x splits into x-x and x-y ordering and that along y splits into y-x and y-y ordering. This splitting depends on the phase difference of coefficients t_a and t_b. However, the ordering J_z remains unchanged. The fictitious magnetic field along x (h_x) splits into x and y; this splitting is dependent on the phase difference between tunneling ($t_{a\lor b}$) and coupling (J_2). The fictitious magnetic field along z (h_z) remains unchanged. A similar effect is seen on the novel correlations with x-z ordering on nearest-neighbor sites splitting into x-z and y-z and z-x splitting into z-x and z-y. These splittings are dependent on the phase difference between $t_{a\lor b}$ and J_2. The complex hopping parameters result in an accumulation of phase with each hop. In the case when a component hops to the nearest-neighbor site and back, no net phase is accumulated and consequently the z ordering terms remain unaffected. In any other hopping, a net phase is obtained, which is proportional to the difference of the complex phases associated with tunneling and coupling. Since this is a one-dimensional system, there is only a trivial effect of these complex coefficients; interesting outcomes are expected at higher dimensions.

Occupancy >1. Considering two particles per site, the two-component Bose-Hubbard system is mapped to a spin-1 system with basis states $|aa\rangle$, $|ab\rangle$, and $|bb\rangle$ mapped to $|1\rangle$, $|0\rangle$, and $|-1\rangle$, respectively. Considering the limit $U \sim U_{ab}$, since only the spin Mott phase ($|0\rangle$) persists for $U \gg U_{ab}$, the effective spin-1 Hamiltonian

$$
\begin{aligned}
H_{\text{eff}} = {} & \mu \sum_i \left(S_i^z\right)^2 - h_z^{(1)} \sum_i S_i^z - h_x^{(1)} \sum_i S_i^x \\
& - J_z \sum_i S_i^z S_{i+1}^z - J_p \sum_i \left(S_i^x S_{i+1}^x + S_i^y S_{i+1}^y\right) \\
& - J_{xz} \sum_i S_i^x S_{i+1}^z + J_{zx} \sum_i S_i^z S_{i+1}^x, \quad (8)
\end{aligned}
$$

where S_i^α are the spin-1 matrices. $\mu = U - U_{ab}$ orders the sites along the spin Mott ($|0\rangle$) phase for $\mu > 0$ and along z ($|1\rangle$ or $|-1\rangle$) for $\mu < 0$. $h_z^{(1)} = \frac{6(t_a^2 - t_b^2)}{U_{ab}}$ and $h_x^{(1)} = \frac{6 J_2 (t_a + t_b)}{U_{ab}}$ act as fictitious magnetic fields polarizing the spins along z and x, respectively. Similar to spin-$\frac{1}{2}$, we note $J_p = \frac{4 t_a t_b}{U_{ab}}$ provides ferromagnetic ordering along x and y and $J_z = 4 \frac{(t_a^2 + t_b^2 - J_2^2)}{U_{ab}}$ provides antiferromagnetic or ferromagnetic ordering along z (dependent on the tunneling and coupling parameters t_a, t_b, and J_2). $J_{xz} = \frac{4 J_2 t_a}{U_{ab}}$ and $J_{zx} = \frac{4 J_2 t_b}{U_{ab}}$ provide the novel ordering along x-z and z-x on nearest-neighbor sites. As expected, despite increasing the occupancy, the novel ordering persists. In the spin-1 system, an additional competing parameter μ appears with an additional spin Mott phase.

Generalizing to spin $S = \frac{M}{2}$ for occupancy M, the effective spin-S Hamiltonian (S_i^α are spin S matrices) (Appendix D)

$$
\begin{aligned}
H_{\text{eff}} = {} & \mu \sum_i \left(S_i^z\right)^2 - h_z^{(S)} \sum_i S_i^z - h_x^{(S)} \sum_i S_i^x \\
& - J_z \sum_i S_i^z S_{i+1}^z - J_p \sum_i \left(S_i^x S_{i+1}^x + S_i^y S_{i+1}^y\right) \\
& - J_{xz} \sum_i S_i^x S_{i+1}^z + J_{zx} \sum_i S_i^z S_{i+1}^x, \quad (9)
\end{aligned}
$$

where $h_z^{(S)} = 2(2S+1)\frac{(t_a^2 - t_b^2)}{U_{ab}}$ and $h_x^{(S)} = 2(2S+1)\frac{J_2(t_a + t_b)}{U_{ab}}$.

VII. SUMMARY

In conclusion, coupling of the two components in the nearest-neighbor sites via a resonant two-photon Raman transition gives rise to a new effective spin Hamiltonian and a unique site-dependent non-FM spin phase. The signature of this unique phase appears as an oscillation in spatial z-x correlation between spins at site 1 and some site j, whereas it remains constant (≈ 0) in a conventional zAFM spin phase. The phase space notably changes with the introduction of coupling, changing the previously seen first-order phase transition between the FM and non-FM (zAFM) spin phases to a second-order phase transition for $U \gg U_{ab}$. The corresponding transition width increases with $\frac{J_2}{t_a}$. For $U \sim U_{ab}$, the system goes from having only one (FM) spin phase to two phases (FM and non-FM) with a second-order phase transition between the two. Our analysis demonstrates that coupling of the components in the nearest-neighbor sites provides an easily tunable parameter to switch between the previously

seen zAFM, zFM, and xFM spin phases allowing for the implementation of a spin-independent optical lattice.

We employ exact diagonalization for small system size ($N < 14$) and variational Monte Carlo with stochastic minimization on the entangled-plaquette state for large system size ($N \geqslant 14$). These confirm the presence of strong unconventional correlations beyond the mean-field approximation. Introduction of complex intracomponent tunneling and intercomponent coupling alters the ordering along x. The unconventional correlations split to have x and y spin orders on a site and z on its nearest-neighbor sites. For filling factor greater than unity, we present the effective spin Hamiltonian in the presence of coupling and demonstrate that the novel correlations persist, and also granting the possibility of transitioning between the different spin phases via the coupling instead of the on-site interactions.

Future avenues. Our work provides new insights into the Bose-Hubbard model and offers an easily tunable phase parameter. The system with coupling can be investigated for symmetry protected topological (SPT) phases [100]. A possible extension to two tilted 1D optical lattices parallel to each other can obtain the Su-Schrieffer-Heeger (SSH) model and develop a SPT phase by tuning the coupling and tunneling parameters. Going to higher dimensions, new rich physics is expected [101]. Our assessment of the mapped system with complex hopping coefficients leads to the system acquiring a phase with second-order hopping. This is extendable to higher dimensions, where the phase acquired over hopping can have far more interesting consequences: development of Harper's Hamiltonian [97] and interesting spin correlations in the mapped effective spin Hamiltonian. Additionally, the effect of the unconventional correlations for a generalized M occupancy at even and odd fillings using the mapped spin-$\frac{M}{2}$ Hamiltonian can be studied. In the absence of coupling, a spin-1 system mapped from a two-component Bose-Hubbard model with occupancy 2 is used to lower entropy and obtain ultracold temperature [95]; this motivates the consideration of occupancy greater than 1. The tunability of the system via coupling can provide additional control over the system at higher occupancy. Rydberg atoms have garnered immense relevance for demonstrating interesting phases and system behavior with their long-range van der Waals interactions leading to blockade [102], and the resonant dipole-dipole interaction [100]. Finally, unexpected spin behaviors may emerge when incorporating Rydberg atoms on account of their interesting properties.

APPENDIX A: EFFECTIVE HAMILTONIAN: CANONICAL TRANSFORMATION

Define two complementary subspaces: $H_{\mathcal{P}}$ (low-energy) with projector $\mathcal{P}$ and H_Q (high-energy) with projector $Q (= 1 - \mathcal{P})$. The effective Hamiltonian (up to second order) can

be expressed as [103]

$$H_{\text{eff}} = \mathcal{P}H\mathcal{P} - \mathcal{P}HQ\frac{1}{QHQ}QH\mathcal{P}. \quad (A1)$$

The zeroth order has no contribution as the hopping terms in the Hamiltonian lead to higher occupancy and are thus projected out. The interaction terms yield 0 for unit occupancy. In $\mathcal{P}HQ$ or $QH\mathcal{P}$ the only contribution is from hopping terms (t_a, t_b, J_2) in the Hamiltonian that can couple the two subspaces, while in QHQ, only the interaction terms (U, U_{ab}) contribute as they do not change the subspace.

The second-order term $\mathcal{P}HQ\frac{1}{QHQ}QH\mathcal{P}$ is

$$= \mathcal{P}\left[\sum_i(-t_a a_i^\dagger a_{i+1} - t_b b_i^\dagger b_{i+1} + \text{H.c.}) - J_2(b_i^\dagger a_{i+1} + a_{i+1}^\dagger b_i)\right]Q\left(1\Big/\left\{Q\left[\sum_{k=a,b;i}\frac{U_k}{2}n_{ki}(n_{ki}-1) + \sum_i U_{ab}n_{ai}n_{bi}\right]Q\right\}\right)$$

$$\times Q\left[\sum_i(-t_a a_i^\dagger a_{i+1} - t_b b_i^\dagger b_{i+1} + \text{H.c.}) - J_2(b_i^\dagger a_{i+1} + a_{i+1}^\dagger b_i)\right]\mathcal{P}. \quad (A2)$$

There are nine second-order or virtual hopping processes that contribute to and form the effective Hamiltonian. The first and second describe two particles of the same component exchanging positions. The eighth and ninth are when component b (or a) hops from $(i+1) \vee (i-1)$ to i and component a (or b) hops from i to $(i+1) \vee (i-1)$. These four processes have been studied previously [39] and result in xyFM and either zAFM or FM phases. With the introduction of J_2, five additional processes arise. The third process describes component a at $i+1$ and b at i exchanging positions. The fourth and sixth together represent $(a \vee b)_i, a_{i+1} \to b_i, (a \vee b)_{i+1}$. Similarly, the fifth and seventh together describe $b_i, (a \vee b)_{i+1} \to (a \vee b)_i, a_{i+1}$. These processes are derived and expressed as follows:

$$①\frac{1}{QHQ}\mathcal{P}\sum_i -t_a(a_{i+1}^\dagger + a_{i-1}^\dagger)a_i Q\sum_i -t_a a_i^\dagger(a_{i+1} + a_{i-1})\mathcal{P}$$

$$= \frac{t_a^2}{U_{ab}}\sum_i \mathcal{P}(n_{a,i+1} + n_{a,i-1})(a_i n_{b,i} a_i^\dagger)\mathcal{P} + \frac{t_a^2}{U}\sum_i \mathcal{P}(n_{a,i+1} + n_{a,i-1})[a_i(1 - n_{b,i})a_i^\dagger]\mathcal{P}$$

$$= \frac{t_a^2}{U_{ab}}\sum_i \left(\frac{I + \sigma_{i+1}^z}{2} + \frac{I + \sigma_{i-1}^z}{2}\right)\left(\frac{I - \sigma_i^z}{2}\right) + \frac{t_a^2}{U}\sum_i \left(\frac{I + \sigma_{i+1}^z}{2} + \frac{I + \sigma_{i-1}^z}{2}\right)(I + \sigma_i^z)$$

$$= \frac{t_a^2}{2U_{ab}}\sum_i \left(I - \sigma_i^z\sigma_{i+1}^z\right) + \frac{t_a^2}{U}\sum_i \left(I + 2\sigma_i^z + \sigma_i^z\sigma_{i+1}^z\right),$$

$$②\frac{1}{QHQ}\mathcal{P}\sum_i -t_b(b_{i+1}^\dagger + b_{i-1}^\dagger)b_i Q\sum_i -t_b b_i^\dagger(b_{i+1} + b_{i-1})\mathcal{P}$$

$$= \frac{t_b^2}{2U_{ab}}\sum_i \left(I - \sigma_i^z\sigma_{i+1}^z\right) + \frac{t_b^2}{U}\sum_i \left(I - 2\sigma_i^z + \sigma_i^z\sigma_{i+1}^z\right),$$

$$③\frac{1}{QHQ}\mathcal{P}\sum_i -J_2(a_{i+1}^\dagger b_i + b_{i-1}^\dagger a_i)Q\sum_i -J_2(b_i^\dagger a_{i+1} + a_i^\dagger b_{i-1})\mathcal{P}$$

$$= \frac{J_2^2}{QHQ}\sum_i \mathcal{P}(n_{a,i+1}b_i Q b_i^\dagger + n_{b,i-1}a_i Q a_i^\dagger)\mathcal{P}$$

$$= \sum_i \left[\frac{J_2^2}{U}\mathcal{P}n_{a,i+1}(1 + n_{b,i})(1 - n_{a,i}) + n_{b,i-1}(1 + n_{a,i})(1 - n_{b,i})\mathcal{P}\right.$$

$$\left. + \frac{J_2^2}{U_{ab}}\mathcal{P}n_{a,i+1}(1 + n_{b,i})n_{a,i} + n_{b,i-1}(1 + n_{a,i})n_{b,i}\mathcal{P}\right]$$

$$= \frac{J_2^2}{U}\sum_i \left(I - \sigma_i^z\sigma_{i+1}^z\right) + \frac{J_2^2}{2U_{ab}}\sum_i \left(I + \sigma_i^z\sigma_{i+1}^z\right).$$

The fourth and fifth processes together contribute to the fictitious magnetic field h_x and novel correlation J_{xz}:

$$④\frac{1}{QHQ}\mathcal{P}\sum_i -t_a(a_{i+1}^\dagger + a_{i-1}^\dagger)a_i Q\sum_i -J_2(b_i^\dagger a_{i+1} + a_i^\dagger b_{i-1})\mathcal{P}$$

$$= \frac{J_2 t_a}{U_{ab}}\sum_i \mathcal{P}(n_{a,i+1}b_i^\dagger a_i + a_{i-1}^\dagger b_{i-1}a_i n_{b,i} a_i^\dagger)\mathcal{P} + \frac{J_2 t_a}{U}\sum_i \mathcal{P}a_{i-1}^\dagger b_{i-1}a_i(1 - n_{b,i})a_i^\dagger \mathcal{P}$$

$$= \frac{J_2 t_a}{2U_{ab}} \sum_i (\sigma_i^x - i\sigma_i^y \sigma_{i+1}^z) + \frac{J_2 t_a}{2U} \sum_i (\sigma_{i-1}^x + i\sigma_{i-1}^y + \sigma_i^z \sigma_{i-1}^x + i\sigma_i^z \sigma_{i-1}^y),$$

⑤ $$\frac{1}{QHQ} \mathcal{P} \sum_i -J_2(a_{i+1}^\dagger b_i + b_{i-1}^\dagger a_i) Q \sum_i -t_a a_i^\dagger (a_{i+1} + a_{i-1}) \mathcal{P}$$

$$= \frac{J_2 t_a}{QHQ} \sum_i \mathcal{P}(n_{a,i+1} b_i Q a_i^\dagger + b_{i-1}^\dagger a_{i-1} a_i Q a_i^\dagger) \mathcal{P}$$

$$= \frac{J_2 t_a}{2U_{ab}} \sum_i (\sigma_i^x + i\sigma_i^y \sigma_{i+1}^z) + \frac{J_2 t_a}{2U} \sum_i (\sigma_{i-1}^x - i\sigma_{i-1}^y + \sigma_i^z \sigma_{i-1}^x - i\sigma_i^z \sigma_{i-1}^y).$$

The sixth and seventh processes together contribute to the fictitious magnetic field h_x and novel correlation J_{zx}:

⑥ $$\frac{1}{QHQ} \mathcal{P} \sum_i -t_b(b_{i+1}^\dagger + b_{i-1}^\dagger) b_i Q \sum_i -J_2(b_i^\dagger a_{i+1} + a_i^\dagger b_{i-1}) \mathcal{P}$$

$$= \frac{J_2 t_b}{QHQ} \sum_i \mathcal{P}(n_{b,i-1} b_i Q a_i^\dagger + b_{i+1}^\dagger a_{i+1} b_i Q b_i^\dagger) \mathcal{P}$$

$$= \frac{J_2 t_b}{2U_{ab}} \sum_i (\sigma_i^x - i\sigma_i^y \sigma_{i-1}^z) + \frac{J_2 t_b}{2U} \sum_i \sigma_{i+1}^x - i\sigma_{i+1}^y - \sigma_i^z \sigma_{i+1}^x + i\sigma_i^z \sigma_{i+1}^y,$$

⑦ $$\frac{1}{QHQ} \mathcal{P} \sum_i -J_2(a_{i+1}^\dagger b_i + b_{i-1}^\dagger a_i) Q \sum_i -t_b b_i^\dagger (b_{i+1} + b_{i-1}) \mathcal{P}$$

$$= \frac{J_2 t_b}{QHQ} \sum_i \mathcal{P}(n_{b,i-1} a_i Q b_i^\dagger + a_{i+1}^\dagger b_{i+1} b_i Q b_i^\dagger) \mathcal{P}$$

$$= \frac{J_2 t_b}{2U_{ab}} \sum_i (\sigma_i^x + i\sigma_i^y \sigma_{i-1}^z) + \frac{J_2 t_b}{2U} \sum_i \sigma_{i+1}^x + i\sigma_{i+1}^y - \sigma_i^z \sigma_{i+1}^x - i\sigma_i^z \sigma_{i+1}^y,$$

⑧ $$\frac{1}{QHQ} \mathcal{P} \sum_i -t_a(a_{i+1}^\dagger + a_{i-1}^\dagger) a_i Q \sum_i -t_b b_i^\dagger (b_{i+1} + b_{i-1}) \mathcal{P}$$

$$= \frac{t_a t_b}{4U_{ab}} \sum_i \left[(\sigma_{i+1}^x + i\sigma_{i+1}^y)(\sigma_i^x - i\sigma_i^y) + (\sigma_{i-1}^x + i\sigma_{i-1}^y)(\sigma_i^x - i\sigma_i^y) \right]$$

$$= \frac{t_a t_b}{2U_{ab}} \sum_i (\sigma_i^x \sigma_{i+1}^x + \sigma_i^y \sigma_{i+1}^y),$$

⑨ $$\frac{1}{QHQ} \mathcal{P} \sum_i -t_b(b_{i+1}^\dagger + b_{i-1}^\dagger) b_i Q \sum_i -t_a a_i^\dagger (a_{i+1} + a_{i-1}) \mathcal{P}$$

$$= \frac{t_a t_b}{2U_{ab}} \sum_i (\sigma_i^x \sigma_{i+1}^x + \sigma_i^y \sigma_{i+1}^y).$$

Then, the second term ($\mathcal{P}HQ\frac{1}{QHQ}QH\mathcal{P}$) in the expansion (A1)

$$= \frac{t_a t_b}{U_{ab}} \sum_i (\sigma_i^x \sigma_{i+1}^x + \sigma_i^y \sigma_{i+1}^y) + (t_a^2 + t_b^2 - J_2^2) \left(\frac{1}{U} - \frac{1}{2U_{ab}} \right) \sum_i \sigma_i^z \sigma_{i+1}^z + 2\frac{t_a^2 - t_b^2}{U} \sum_i \sigma_i^z + J_2(t_a + t_b) \left(\frac{1}{U} + \frac{1}{U_{ab}} \right) \sum_i \sigma_i^x$$

$$- \frac{J_2 t_b}{U} \sum_i \sigma_i^z \sigma_{i+1}^x + \frac{J_2 t_a}{U} \sum_i \sigma_i^x \sigma_{i+1}^z. \tag{A3}$$

Finally, the effective spin Hamiltonian

$$H_{\text{eff}} = \sum_i \left[-J_\perp (\sigma_i^x \sigma_{i+1}^x + \sigma_i^y \sigma_{i+1}^y) - J_z \sigma_i^z \sigma_{i+1}^z - h_z(\sigma_i^z) - h_x(\sigma_i^x) + J_{zx} \sigma_i^z \sigma_{i+1}^x - J_{xz} \sigma_i^x \sigma_{i+1}^z \right]. \tag{A4}$$

APPENDIX B: $N = 2$

The aim here is to investigate a simplified two-site system as it provides a facile description allowing for the validation of

the effective spin system, by comparing the ground states of the original with the mapped two-component Bose-Hubbard Hamiltonian. Consider two sites each hosting component $a \vee$
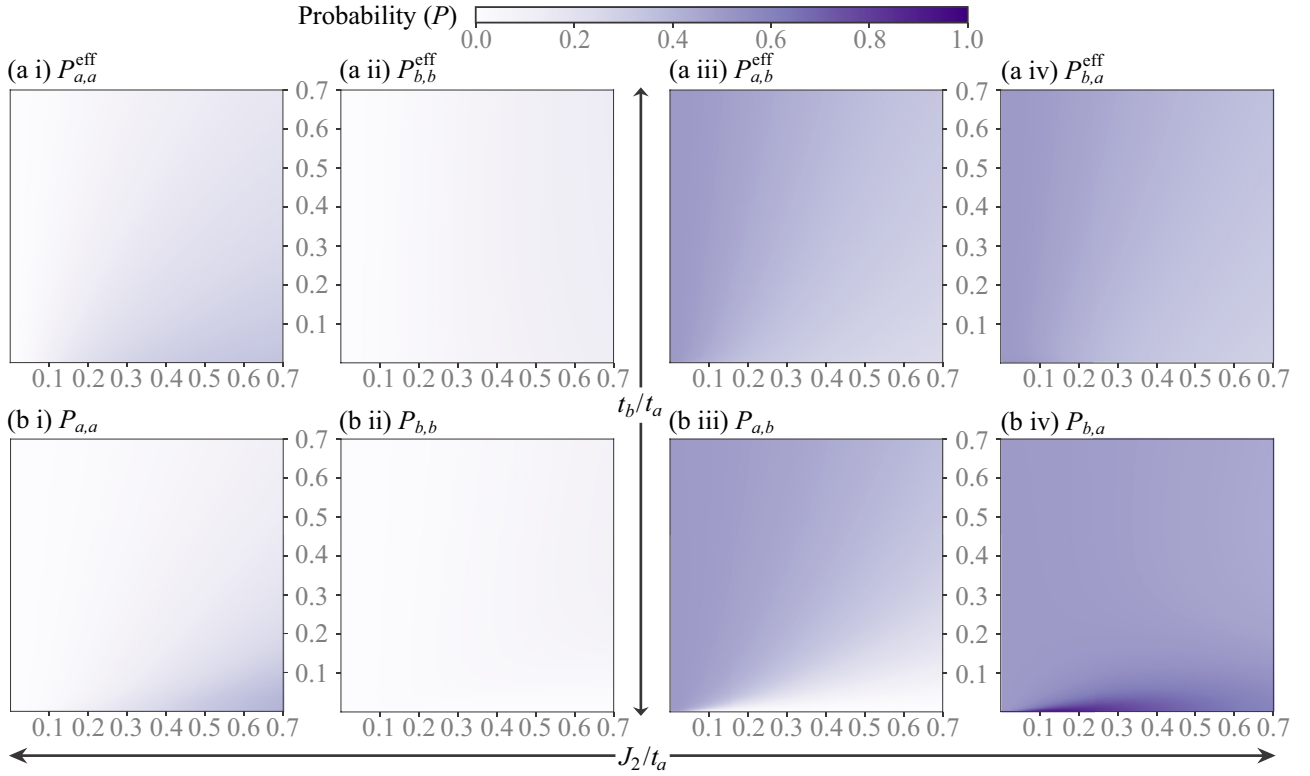
FIG. 7. Probability of the basis states of the (a) effective Hamiltonian and (b) low-energy basis states of the original Hamiltonian (i) $|a\rangle_1 |a\rangle_2$, (ii) $|b\rangle_1 |b\rangle_2$, (iii) $|a\rangle_1 |b\rangle_2$, and (iv) $|b\rangle_1 |a\rangle_2$. The probabilities are determined in the deep Mott regime ($\frac{U_{ab}}{t_a} = 20$) $\frac{U}{U_{ab}} = 10$ and presented as a function of scaled tunneling ($\frac{t_b}{t_a}$) and coupling ($\frac{J_2}{t_a}$).

b, forming the basis states $|a\rangle_1 |a\rangle_2$, $|a\rangle_1 |b\rangle_2$, $|b\rangle_1 |a\rangle_2$, and $|b\rangle_1 |b\rangle_2$ with the analysis restricted to the limit $U \gg U_{ab}$. The coupling and the tunneling couple these basis states in the original system to high-energy states $|aa\rangle_1 |0\rangle_2$, $|0\rangle_1 |aa\rangle_2$, $|ab\rangle_1 |0\rangle_2$, $|0\rangle_1 |ab\rangle_2$, $|bb\rangle_1 |0\rangle_2$, and $|0\rangle_1 |bb\rangle_2$. The effective spin Hamiltonian and the original Hamiltonian are studied via exact diagonalization with open boundary conditions. In Fig. 7(a), the ground state of the mapped effective spin system is presented as a function of coupling ($\frac{J_2}{t_a}$) and tunneling ($\frac{t_b}{t_a}$). Upon comparison of the mapped spin system with the ground state of the original system in Fig. 7(b) (low-energy subspace), both systems show a similar ground state composition as a function of tunneling and coupling. At large coupling ($\frac{J_2}{t_a} \gg \frac{t_b}{t_a}$) the ground state compositions of the two systems deviate, where the mapped system shows a lower probability of the state $|b\rangle_1 |a\rangle_2$ and thus higher probability of the other three basis states. At higher values of coupling, the Mott condition required for the mapping fails. This leads to a negligible but nonzero probability of high-energy states $|aa\rangle_1 |0\rangle_2$, $|0\rangle_1 |aa\rangle_2$, $|ab\rangle_1 |0\rangle_2$, $|0\rangle_1 |ab\rangle_2$, $|bb\rangle_1 |0\rangle_2$, and $|0\rangle_1 |bb\rangle_2$. Additionally, the mapped effective Hamiltonian works best for a large system size and in the derivation of the effective Hamiltonian the expansion is limited to second order; inclusion of higher-order terms can reduce the deviation seen in the ground state composition between the mapped and original system. Studying the probability of basis states, we confirm that the mapped system is an appropriate representation for the parameter strengths considered. We explain the ground state of mapped system by studying the effective Hamiltonian.

The preference for $|b\rangle_1 |a\rangle_2$ appears due to $J_z \propto J_2$, and for $|a\rangle_1 |a\rangle_2$ or $|b\rangle_1 |b\rangle_2$ due to the ordering $J_z, h_z \propto t_{a\vee b}$, whereas the preference for the superposition of states $|a\rangle_1 |a\rangle_2$ and $|b\rangle_1 |a\rangle_2$ or $|b\rangle_1 |b\rangle_2$ and $|b\rangle_1 |a\rangle_2$ emerges due to J_{zx} or J_{xz}. For the interaction limit $U \sim U_{ab}$, a similar conclusion can be made.

APPENDIX C: ANALYTICAL PHASE BOUNDARY

Within the mean-field approximation, with the variational ansatz defined, the energy per site

$$E_{\mathrm{MF}} = -J_z \cos 2\theta_A \cos 2\theta_B - J_p \sin 2\theta_A \sin 2\theta_B$$
$$- \frac{h_z}{2}(\cos 2\theta_A + \cos 2\theta_B) - \frac{h_x}{2}(\sin 2\theta_A + \sin 2\theta_B)$$
$$- \frac{(J_{xz} - J_{zx})}{2}(\cos 2\theta_A \sin 2\theta_B + \sin 2\theta_A \cos 2\theta_B).$$

Minimizing energy with respect to θ_B ($\frac{\partial E}{\partial \theta_B} = 0$)

$$\sin 2\theta_B = \frac{K_1}{\sqrt{K_1^2 + K_2^2}}, \quad \cos 2\theta_B = \frac{K_2}{\sqrt{K_1^2 + K_2^2}},$$

where $K_1 = J_p \sin 2\theta_A + \frac{(J_{xz} - J_{zx})}{2} \cos 2\theta_A + \frac{h_x}{2}$ and $K_2 = J_z \cos 2\theta_A + \frac{(J_{xz} - J_{zx})}{2} \sin 2\theta_A + \frac{h_z}{2}$.

The energy after eliminating θ_B

$$E_{\mathrm{MF}} = -\frac{1}{2}(h_z \cos 2\theta_A + h_x \sin 2\theta_A) - \sqrt{K_1^2 + K_2^2}.$$

The energy is too complicated to solve for θ_A; approximations are made to obtain analytical expressions for θ_A.

$U \gg U_{ab}$. We consider two approximations. In approximation (i), consider only J_p, J_z, and h_x. This is valid for small and intermediate $\frac{t_b}{t_a}$ and $\frac{J_2}{t_a}$. Under this assumption, the non-FM (NFM) phase is approximately derived from the mean-field energy:

$$E_{\mathrm{MF}} = -\frac{h_x \sin 2\theta_A}{2}$$
$$- \sqrt{\left(J_z^2 - J_p^2\right)\cos^2 2\theta_A + J_p h_x \sin 2\theta_A + J_p^2 + \frac{h_x^2}{4}}.$$

Minimizing energy with respect to θ_A and solving for θ_A,

$$\sin 2\theta_A^{\mathrm{NFM},1\vee2} = \frac{J_p h_x \pm |J_z| h_x}{2\left(J_z^2 - J_p^2\right)}, \quad \sin 2\theta_A^{\mathrm{NFM},3} = 1.$$

$\theta_A^{\mathrm{NFM},1}$ fits the numerically obtained θ_A best among the three in the non-FM region.

In approximation (ii), consider each of the following cases:

(1) J_z, h_x (large $\frac{J_2}{t_a}$ and small $\frac{t_b}{t_a}$) or
(2) J_p, J_z (small $\frac{J_2}{t_a}$ and large $\frac{t_b}{t_a}$) or
(3) J_p, h_x (large $\frac{J_2}{t_a}$ and large $\frac{t_b}{t_a}$),
where the terms are significant. In all three of the cases,

$$\cos 2\theta_A^{\mathrm{FM}} = 0.$$

The critical value of $\frac{t_b}{t_a}$, going from non-FM to FM, obtained by finding the boundary between the two analytical θ_A is computed as follows:

$$\left(\frac{t_b}{t_a}\right)_{U \gg U_{ab}}^C = -\left(\frac{\frac{J_2}{t_a}(U + U_{ab}) + 2U}{2(2U_{ab} - U)}\right) - \sqrt{\left(\frac{\frac{J_2}{t_a}(U + U_{ab}) + 2U}{2(2U_{ab} - U)}\right)^2 - \left(1 - \frac{J_2^2}{t_a^2} + \frac{\frac{J_2}{t_a}(U + U_{ab})}{2U_{ab} - U}\right)}.$$

$U \sim U_{ab}$. We consider two approximations. In approximation (i), set h_z and $J_{xz} - J_{zx}$ to 0. This is valid when the intracomponent tunnelings are small ($t_b, t_a \ll J_2$), or comparable to each other ($t_a \sim t_b$). This limit is able to approximately capture the non-FM phase from the mean-field energy:

$$E_{\mathrm{MF}} = -\frac{h_x \sin 2\theta_A}{2} - \sqrt{\left(J_z^2 - J_p^2\right)\cos^2 2\theta_A + J_p h_x \sin 2\theta_A + J_p^2 + \frac{h_x^2}{4}}.$$

Minimizing energy with respect to θ_A and solving for θ_A:

$$\sin 2\theta_A^{\mathrm{NFM},1\vee2} = \frac{J_p h_x \pm |J_z| h_x}{2\left(J_z^2 - J_p^2\right)}, \quad \sin 2\theta_A^{\mathrm{NFM},3} = 1.$$

$\theta_A^{\mathrm{NFM},1}$ fits the numerically obtained θ_A best among the three in the non-FM region.

In approximation (ii), set J_z, J_p, and $J_{xz} - J_{zx}$ to 0. This solution set only considers the spin-polarizing terms h_z and h_x, and is able to capture the FM phase. This approximation is valid for small coupling $\frac{J_2}{t_a}$. It however fails to capture the region around $\frac{t_b}{t_a} \sim 1$ and $\frac{J_2}{t_a} \to 0$, where both the ordering terms considered would tend to 0:

$$E_{\mathrm{MF}} = -\frac{h_z \cos 2\theta_A}{2} - \frac{h_x \sin 2\theta_A}{2} - \sqrt{\frac{h_z^2 + h_x^2}{4}}.$$

Minimizing energy with respect to θ_A and solving for θ_A,

$$\cos 2\theta_A^{\mathrm{FM}} = \frac{h_z}{\sqrt{h_z^2 + h_x^2}}.$$

The critical value of $\frac{t_b}{t_a}$, going from non-FM to FM, obtained by finding the boundary between the two analytical θ_A is computed ($\theta_A^{\mathrm{NFM},1} = \lim_{h_z \to 0} \theta_A^{\mathrm{FM}} = \frac{\pi}{4}$) as follows:

$$\left(\frac{t_b}{t_a}\right)_{U \sim U_{ab}}^C = -\left(\frac{\frac{J_2}{t_a}(U + U_{ab}) + 2U}{2(2U_{ab} - U)}\right) + \sqrt{\left(\frac{\frac{J_2}{t_a}(U + U_{ab}) + 2U}{2(2U_{ab} - U)}\right)^2 - \left(1 - \frac{J_2^2}{t_a^2} + \frac{\frac{J_2}{t_a}(U + U_{ab})}{2U_{ab} - U}\right)}.$$

APPENDIX D: MAPPING M PARTICLES PER SITE

Generalizing the system to M particles per site, with the analysis limited to $U - U_{ab} = \mu \ll U, U_{ab}$, consider a site having n_a particles of component a and n_b of component b, such that $n_a + n_b = M$. To map the two-component Bose-Hubbard model to an effective low-energy Hamiltonian, define the subspaces P (occupancy $= M$) and Q (occupancy $> M$).

The effective Hamiltonian up to second-order

$$H_{\text{eff}} = PHP - PHQ\frac{1}{QHQ - PHP}QHP.$$

Mapping the bosonic creation, annihilation, and number operators to spin-$\frac{M}{2}$ matrices,

$$n_{a,i} = \frac{M}{2} + S_i^z, \quad n_{b,i} = \frac{M}{2} - S_i^z, \quad a_i^\dagger b_i = S_i^x + iS_i^y, \quad b_i^\dagger a_i = S_i^x - iS_i^y.$$

The first term in the Hamiltonian

$$PHP = \frac{U}{2}n_{a,i}(n_{a,i} - 1) + \frac{U}{2}n_{b,i}(n_{b,i} - 1) + U_{ab}n_{a,i}n_{b,i} = \frac{U}{2}M(M - 1) - \mu\frac{M^2}{4} + \mu\left(S_i^z\right)^2.$$

The second term in the Hamiltonian, $-PHQ\frac{1}{QHQ-PHP}QHP$, is split into 4 terms:

(a) $\quad -t_a^2 P\left[(n_{a,i+1} + n_{a,i-1})a_i\frac{Q}{QHQ - PHP}a_i^\dagger\right]P - t_b^2 P\left[(n_{b,i+1} + n_{b,i-1})b_i\frac{Q}{QHQ - PHP}b_i^\dagger\right]P$

$\qquad -J_2^2 P\left[n_{a,i+1}b_i\frac{Q}{QHQ - PHP}b_i^\dagger + n_{b,i-1}a_i\frac{Q}{QHQ - PHP}a_i^\dagger\right]P$

(b) $\quad -t_a t_b P\left[(a_{i+1}^\dagger b_{i+1} + a_{i-1}^\dagger b_{i-1})a_i\frac{Q}{QHQ - PHP}b_i^\dagger + (b_{i+1}^\dagger a_{i+1} + b_{i-1}^\dagger a_{i-1})b_i\frac{Q}{QHQ - PHP}a_i^\dagger\right]P$

(c) $\quad -J_2 t_a P\left[n_{a,i+1}\left(a_i\frac{Q}{QHQ - PHP}b_i^\dagger + b_i\frac{Q}{QHQ - PHP}a_i^\dagger\right) + (a_{i-1}^\dagger b_{i-1} + b_{i-1}^\dagger a_{i-1})a_i\frac{Q}{QHQ - PHP}a_i^\dagger\right]P$

(d) $\quad -J_2 t_b P\left[n_{b,i-1}\left(a_i\frac{Q}{QHQ - PHP}b_i^\dagger + b_i\frac{Q}{QHQ - PHP}a_i^\dagger\right) + (a_{i+1}^\dagger b_{i+1} + b_{i+1}^\dagger a_{i+1})b_i\frac{Q}{QHQ - PHP}b_i^\dagger\right]P.$

Focusing on (a), $QHQ - PHP \approx U_{ab}M$; $a_iQa_i^\dagger$

$$= \sum_{n_b=0}^{M} a_i\left[\prod_{k=0,k\neq n_b}^{N}\frac{(k - n_{b,i})}{(k - n_b)}\right]a_i^\dagger = \sum_{n_b=0}^{M}(n_a + 1)\left[\prod_{k=0,k\neq n_b}^{N}\frac{(k - n_{b,i})}{(k - n_b)}\right]$$

$$= \sum_{n_b=0}^{M}(M + 1 - n_b)\left[\frac{1}{n_b!}\frac{1}{(M - n_b)!}\right]\left[(-1)^{n_b}\prod_{k=0,k\neq n_b}^{M}(k - n_{b,i})\right]$$

$$= \frac{1}{M!}\sum_{n_b=0}^{M}(-1)^{n_b}(M + 1 - n_b)\binom{M}{n_b}\left[\prod_{k=0,k\neq n_b}^{M}(k - n_{b,i})\right].$$

It follows that

$$b_iQb_i^\dagger = \frac{1}{M!}\sum_{n_a=0}^{M}(-1)^{n_a}(M + 1 - n_a)\binom{M}{n_a}\left[\prod_{k=0,k\neq n_a}^{M}(k - n_{a,i})\right].$$

Simplifying the terms in the above expression,

$$\prod_{k=0,k\neq n_b}^{M}(k - n_{b,i}) = C_0 + C_1 n_{b,i} + C_2 n_{b,i}^2 + \ldots + C_M n_{b,i}^M, \quad C_M = (-1)^M, \quad C_{M-1} = (-1)^M n_b + (-1)^{M-1}\left(\sum_{n_1=0}^{M} n_1\right),$$

$$C_{M-2} = (-1)^M n_b^2 + (-1)^{M-1}\left(\sum_{n_1=0}^{M} n_1\right)n_b + (-1)^{M-2}\left(\sum_{\substack{n_1=0 \\ n_2>n_1}}^{M} n_1 n_2\right) + \ldots,$$

$$C_1 = (-1)^M n_b^{M-1} + \ldots, \quad C_0 = (-1)^M n_b^M + (-1)^{M-1}\left(\sum_{n_1=0}^{M} n_1\right)n_b^{M-1} + \ldots,$$

$$C_{M-k} = (-1)^M n_b^k + (-1)^{M-1}\left(\sum_{n_1=0}^{M} n_1\right)n_b^{k-1} + \dots, \quad \sum_{n_b}(-1)^{n_b} n_b^k \binom{M}{n_b} = \begin{cases} (-1)^M M!, & \text{if } k=M, \\ 0, & k < M, \end{cases}$$

$$n_b^M = n_b(n_b-1)(n_b-2)\dots[n_b-(M-1)] + \left(\sum_{n_1=0}^{M-1} n_1\right)n_b^{M-1}.$$

Substituting these simplifications, $a_i Q a_i^\dagger$

$$= \frac{1}{M!}\sum_{n_b=0}^{M}(-1)^{n_b}(M+1-n_b)\binom{M}{n_b}\left[\prod_{k=0,k\neq n_b}^{M}(k-n_{b,i})\right]$$

$$= \frac{1}{M!}\sum_{n_b=0}^{M}(M+1)\left[(-1)^{n_b}\binom{M}{n_b}(-1)^M n_b^M\right] - \frac{1}{M!}\sum_{n_b=0}^{M}n_b(-1)^{n_b}\binom{M}{n_b}\left[(-1)^M n_b^M + (-1)^{M-1}\left(\sum_{n=0}^{M}n\right)n_b^{M-1} + (-1)^M n_b^{M-1}n_{b,i}\right]$$

$$= (M+1) - n_{b,i} - \frac{1}{M!}\sum_{n_b=0}^{M}(-1)^{n_b}\binom{M}{n_b}\left[(-1)^M n_b n_b(n_b-1)\dots\right.$$

$$\left.\dots[n_b-(M-1)] + (-1)^M\left(\sum_{n=0}^{M-1}n\right)n_b^M + (-1)^{M-1}\left(\sum_{n=0}^{M}n\right)n_b^M\right]$$

$$= (M+1) - n_{b,i} - M - \frac{1}{M!}\sum_{n_b=0}^{M}(-1)^{n_b}\binom{M}{n_b}(-1)^M\left(\frac{M(M-1)}{2} - \frac{M(M+1)}{2}\right)n_b^M$$

$$= (M+1) - n_{b,i} - M + M = (M+1) - n_{b,i}.$$

It follows that $b_i Q b_i^\dagger = (M+1) - n_{a,i}$.

Simplifying (a) in the expression (z: number of nearest neighbors),

$$\text{(a)} \quad = -\frac{t_a^2}{MU_{ab}}P[(n_{a,i+1} + n_{a,i-1})(M+1-n_{b,i})]P - \frac{t_b^2}{MU_{ab}}P[(n_{b,i+1} + n_{b,i-1})(M+1-n_{a,i})]P$$

$$- \frac{J_2^2}{MU_{ab}}P[n_{b,i+1}(M+1-n_{b,i}) + n_{a,i-1}(M+1-n_{a,i})]P$$

$$= -\frac{zt_a^2}{MU_{ab}}\left[\text{const.} + (M+1)S_i^z + S_i^z S_{i+1}^z\right] - \frac{zt_b^2}{MU_{ab}}\left[\text{const.} - (M+1)S_i^z + S_i^z S_{i+1}^z\right] + \frac{zJ_2^2}{MU_{ab}}S_i^z S_{i+1}^z.$$

Considering the other terms in the second expression of the effective Hamiltonian [for (b), (c), and (d), $QHQ - PHP = \frac{U}{2}(M-1) + \frac{U_{ab}}{2}(M+1) \approx U_{ab}M$],

$$\text{(b)} \quad = -t_a t_b P\left[(a_{i+1}^\dagger b_{i+1} + a_{i-1}^\dagger b_{i-1})a_i\frac{Q}{QHQ - PHP}b_i^\dagger + (b_{i+1}^\dagger a_{i+1} + b_{i-1}^\dagger a_{i-1})b_i\frac{Q}{QHQ - PHP}a_i^\dagger\right]P$$

$$= -\frac{t_a t_b}{MU_{ab}}P\left[(a_{i+1}^\dagger b_{i+1} + a_{i-1}^\dagger b_{i-1})a_i\left(\sum_{n_a}\prod_{k=0,k\neq n_a}^{M}\frac{(k-n_{a,i})}{(k-n_a)}\right)b_i^\dagger\right.$$

$$\left. + (b_{i+1}^\dagger a_{i+1} + b_{i-1}^\dagger a_{i-1})b_i\left(\sum_{n_b}\prod_{k=0,k\neq n_b}^{M}\frac{(k-n_{b,i})}{(k-n_b)}\right)a_i^\dagger\right]P$$

$$= -\frac{t_a t_b}{MU_{ab}}P\left[(a_{i+1}^\dagger b_{i+1} + a_{i-1}^\dagger b_{i-1})b_i^\dagger a_i\frac{M!}{M!} + (b_{i+1}^\dagger a_{i+1} + b_{i-1}^\dagger a_{i-1})a_i^\dagger b_i\frac{M!}{M!}\right]P$$

$$= -\frac{zt_a t_b}{MU_{ab}}\left[(S_{i+1}^x + iS_{i+1}^y)(S_i^x - iS_i^y) + (S_{i+1}^x - iS_{i+1}^y)(S_i^x + iS_i^y)\right]$$

$$= -\frac{z2t_a t_b}{MU_{ab}}(S_i^x S_{i+1}^x + S_i^y S_{i+1}^y)$$

$$\text{(c)} \quad = -J_2 t_a P\left[n_{a,i+1}\left(a_i\frac{Q}{QHQ - PHP}b_i^\dagger + b_i\frac{Q}{QHQ - PHP}a_i^\dagger\right) + (a_{i-1}^\dagger b_{i-1} + b_{i-1}^\dagger a_{i-1})a_i\frac{Q}{QHQ - PHP}a_i^\dagger\right]P$$

$$= -\frac{J_2 t_a}{MU_{ab}}\left(2S_i^x\right)\left(\frac{M}{2} + S_{i+1}^z\right) - \frac{J_2 t_a}{MU_{ab}}\left(2S_{i-1}^x\right)\left(\frac{M}{2} + 1 + S_i^z\right)$$

$$= -\frac{zJ_2 t_a}{MU_{ab}}\left[(M+1)S_i^x + 2S_i^x S_{i+1}^z\right]$$

$$(d)\quad = -J_2 t_b P\left[n_{b,i-1}\left(a_i\frac{Q}{QHQ - PHP}b_i^\dagger + b_i\frac{Q}{QHQ - PHP}a_i^\dagger\right) + (a_{i+1}^\dagger b_{i+1} + b_{i+1}^\dagger a_{i+1})b_i\frac{Q}{QHQ - PHP}b_i^\dagger\right]P$$

$$= -\frac{J_2 t_b}{MU_{ab}}\left(2S_i^x\right)\left(\frac{M}{2} - S_{i-1}^z\right) - \frac{J_2 t_b}{MU_{ab}}\left(2S_{i+1}^x\right)\left(\frac{M}{2} + 1 - S_i^z\right)$$

$$= -\frac{zJ_2 t_b}{MU_{ab}}\left[(M+1)S_i^x - 2S_i^x S_{i+1}^z\right].$$

The effective Hamiltonian, scaled by $M\ (= 2S)$,

$$H_{\text{eff}} = \mu \sum_i \left(S_i^z\right)^2 - z(2S+1)\sum_i \frac{(t_a^2 - t_b^2)}{U_{ab}}S_i^z - z(2S+1)\sum_i \frac{J_2(t_a + t_b)}{U_{ab}}S_i^x - \frac{2(t_a^2 + t_b^2 - J_2^2)}{U_{ab}}\sum_i S_i^z S_{i+1}^z$$

$$- \frac{4t_a t_b}{U_{ab}}\sum_i \left(S_i^x S_{i+1}^x + S_i^y S_{i+1}^y\right) - \frac{4J_2 t_a}{U_{ab}}\sum_i S_i^x S_{i+1}^z + \frac{4J_2 t_b}{U_{ab}}\sum_i S_i^z S_{i+1}^x.$$

---

[1] I. Bloch, J. Dalibard, and S. Nascimbène, Nat. Phys. **8**, 267 (2012).

[2] M. Lewenstein, A. Sanpera, V. Ahufinger, B. Damski, A. Sen(De), and U. Sen, Adv. Phys. **56**, 243 (2007).

[3] M. Greiner, O. Mandel, T. Esslinger, T. W. Hänsch, and I. Bloch, Nature (London) **415**, 39 (2002).

[4] S. Sachdev, *Quantum Phase Transitions* (Cambridge University Press, Cambridge, 2000).

[5] I. Bloch, J. Dalibard, and W. Zwerger, Rev. Mod. Phys. **80**, 885 (2008).

[6] T. Esslinger, Annu. Rev. Condens. Matter Phys. **1**, 129 (2010).

[7] C. Weitenberg, M. Endres, J. F. Sherson, M. Cheneau, P. Schauß, T. Fukuhara, I. Bloch, and S. Kuhr, Nature (London) **471**, 319 (2011).

[8] D. Jaksch, C. Bruder, J. I. Cirac, C. W. Gardiner, and P. Zoller, Phys. Rev. Lett. **81**, 3108 (1998).

[9] O. Morsch and M. Oberthaler, Rev. Mod. Phys. **78**, 179 (2006).

[10] D. C. McKay and B. DeMarco, Rep. Prog. Phys. **74**, 054401 (2011).

[11] B. Capogrosso-Sansone, Ş. G. Söyler, N. V. Prokof'ev, and B. V. Svistunov, Phys. Rev. A **81**, 053622 (2010).

[12] R. Jördens, L. Tarruell, D. Greif, T. Uehlinger, N. Strohmaier, H. Moritz, T. Esslinger, L. De Leo, C. Kollath, A. Georges, V. Scarola, L. Pollet, E. Burovski, E. Kozik, and M. Troyer, Phys. Rev. Lett. **104**, 180401 (2010).

[13] S. Fölling, S. Trotzky, P. Cheinet, M. Feld, R. Saers, A. Widera, T. Müller, and I. Bloch, Nature (London) **448**, 1029 (2007).

[14] T.-L. Ho and Q. Zhou, Phys. Rev. Lett. **99**, 120404 (2007).

[15] P. Medley, D. M. Weld, H. Miyake, D. E. Pritchard, and W. Ketterle, Phys. Rev. Lett. **106**, 195301 (2011).

[16] P. Rabl, A. J. Daley, P. O. Fedichev, J. I. Cirac, and P. Zoller, Phys. Rev. Lett. **91**, 110403 (2003).

[17] S. Trebst, U. Schollwöck, M. Troyer, and P. Zoller, Phys. Rev. Lett. **96**, 250402 (2006).

[18] A. Kantian, A. J. Daley, and P. Zoller, Phys. Rev. Lett. **104**, 240406 (2010).

[19] M. Lubasch, V. Murg, U. Schneider, J. I. Cirac, and M.-C. Bañuls, Phys. Rev. Lett. **107**, 165301 (2011).

[20] A. S. Sørensen, E. Altman, M. Gullans, J. V. Porto, M. D. Lukin, and E. Demler, Phys. Rev. A **81**, 061603(R) (2010).

[21] S. Gammelmark and A. Eckardt, New J. Phys. **15**, 033028 (2013).

[22] J. Dalibard, F. Gerbier, G. Juzeliūnas, and P. Öhberg, Rev. Mod. Phys. **83**, 1523 (2011).

[23] N. Goldman, G. Juzeliūnas, P. Öhberg, and I. B. Spielman, Rep. Prog. Phys. **77**, 126401 (2014).

[24] G.-B. Jo, Y.-R. Lee, J.-H. Choi, C. A. Christensen, T. H. Kim, J. H. Thywissen, D. E. Pritchard, and W. Ketterle, Science **325**, 1521 (2009).

[25] J. Struck, C. Ölschläger, R. Le Targat, P. Soltan-Panahi, A. Eckardt, M. Lewenstein, P. Windpassinger, and K. Sengstock, Science **333**, 996 (2011).

[26] A. Eckardt, C. Weiss, and M. Holthaus, Phys. Rev. Lett. **95**, 260404 (2005).

[27] S. Sachdev, K. Sengupta, and S. M. Girvin, Phys. Rev. B **66**, 075128 (2002).

[28] J. Simon, W. S. Bakr, R. Ma, M. E. Tai, P. M. Preiss, and M. Greiner, Nature (London) **472**, 307 (2011).

[29] S. Pielawa, T. Kitagawa, E. Berg, and S. Sachdev, Phys. Rev. B **83**, 205135 (2011).

[30] M. P. A. Fisher, P. B. Weichman, G. Grinstein, and D. S. Fisher, Phys. Rev. B **40**, 546 (1989).

[31] M. Lewenstein, A. Sanpera, and V. Ahufinger, *Ultracold Atoms in Optical Lattices* (Oxford University Press, Oxford, 2012).

[32] A. Aspuru-Guzik and P. Walther, Nat. Phys. **8**, 285 (2012).

[33] R. Blatt and C. F. Roos, Nat. Phys. **8**, 277 (2012).

[34] J. I. Cirac and P. Zoller, Nat. Phys. **8**, 264 (2012).

[35] P. Hauke, F. M. Cucchietti, L. Tagliacozzo, I. Deutsch, and M. Lewenstein, Rep. Prog. Phys. **75**, 082401 (2012).

[36] A. A. Houck, H. E. Türeci, and J. Koch, Nat. Phys. **8**, 292 (2012).

[37] C. Gross and I. Bloch, Science **357**, 995 (2017).

[38] A. B. Kuklov and B. V. Svistunov, Phys. Rev. Lett. **90**, 100401 (2003).

[39] E. Altman, W. Hofstetter, E. Demler, and M. D. Lukin, New J. Phys. **5**, 113 (2003).

[40] J. J. García-Ripoll, M. A. Martin-Delgado, and J. I. Cirac, Phys. Rev. Lett. **93**, 250405 (2004).

[41] E. G. Dalla Torre, E. Berg, and E. Altman, Phys. Rev. Lett. **97**, 260401 (2006).

[42] E. Berg, E. G. Dalla Torre, T. Giamarchi, and E. Altman, Phys. Rev. B **77**, 245119 (2008).

[43] L. Amico, G. Mazzarella, S. Pasini, and F. S. Cataliotti, New J. Phys. **12**, 013002 (2010).

[44] M. Dalmonte, M. Di Dio, L. Barbiero, and F. Ortolani, Phys. Rev. B **83**, 155110 (2011).

[45] D. Rossini and R. Fazio, New J. Phys. **14**, 065012 (2012).

[46] C. Trefzger, C. Menotti, and M. Lewenstein, Phys. Rev. A **78**, 043604 (2008).

[47] X.-F. Zhou, Z.-X. Chen, Z.-W. Zhou, Y.-S. Zhang, and G.-C. Guo, Phys. Rev. A **81**, 021602(R) (2010).

[48] J. Jin, D. Rossini, R. Fazio, M. Leib, and M. J. Hartmann, Phys. Rev. Lett. **110**, 163605 (2013).

[49] T. Mishra, R. V. Pai, S. Ramanan, M. S. Luthra, and B. P. Das, Phys. Rev. A **80**, 043614 (2009).

[50] M. Kumar, S. Sarkar, and S. Ramasesha, Int. J. Mod. Phys. B **25**, 159 (2011).

[51] R. Bai, D. Gaur, H. Sable, S. Bandyopadhyay, K. Suthar, and D. Angom, Phys. Rev. A **102**, 043309 (2020).

[52] D. M. Stamper-Kurn, M. R. Andrews, A. P. Chikkatur, S. Inouye, H.-J. Miesner, J. Stenger, and W. Ketterle, Phys. Rev. Lett. **80**, 2027 (1998).

[53] D. M. Stamper-Kurn and M. Ueda, Rev. Mod. Phys. **85**, 1191 (2013).

[54] K. V. Krutitsky and R. Graham, Phys. Rev. A **70**, 063610 (2004).

[55] T. Kimura, S. Tsuchiya, and S. Kurihara, Phys. Rev. Lett. **94**, 110403 (2005).

[56] Q. Zhou, J. V. Porto, and S. Das Sarma, Phys. Rev. B **83**, 195106 (2011).

[57] J. Pietraszewicz, T. Sowiński, M. Brewczyk, J. Zakrzewski, M. Lewenstein, and M. Gajda, Phys. Rev. A **85**, 053638 (2012).

[58] X. Li, Z. Zhang, and W. V. Liu, Phys. Rev. Lett. **108**, 175302 (2012).

[59] T. Sowiński, M. Łącki, O. Dutta, J. Pietraszewicz, P. Sierant, M. Gajda, J. Zakrzewski, and M. Lewenstein, Phys. Rev. Lett. **111**, 215302 (2013).

[60] L.-M. Duan, E. Demler, and M. D. Lukin, Phys. Rev. Lett. **91**, 090402 (2003).

[61] D. Giuliano, D. Rossini, P. Sodano, and A. Trombettoni, Phys. Rev. B **87**, 035104 (2013).

[62] S. Powell, Phys. Rev. A **79**, 053614 (2009).

[63] A. Hubener, M. Snoek, and W. Hofstetter, Phys. Rev. B **80**, 245109 (2009).

[64] Y. Nakano, T. Ishima, N. Kobayashi, T. Yamamoto, I. Ichinose, and T. Matsui, Phys. Rev. A **85**, 023617 (2012).

[65] G. Thalhammer, G. Barontini, L. De Sarlo, J. Catani, F. Minardi, and M. Inguscio, Phys. Rev. Lett. **100**, 210402 (2008).

[66] J. Klinder, H. Keßler, M. R. Bakhtiari, M. Thorwart, and A. Hemmerich, Phys. Rev. Lett. **115**, 230403 (2015).

[67] R. Landig, L. Hruby, N. Dogra, M. Landini, R. Mottl, T. Donner, and T. Esslinger, Nature (London) **532**, 476 (2016).

[68] C. Kollath, A. Sheikhan, S. Wolff, and F. Brennecke, Phys. Rev. Lett. **116**, 060401 (2016).

[69] F. Mivehvar, H. Ritsch, and F. Piazza, Phys. Rev. Lett. **118**, 073602 (2017).

[70] A. Sheikhan and C. Kollath, Phys. Rev. A **99**, 053611 (2019).

[71] F. Schlawin, A. Cavalleri, and D. Jaksch, Phys. Rev. Lett. **122**, 133602 (2019).

[72] F. Schlawin and D. Jaksch, Phys. Rev. Lett. **123**, 133601 (2019).

[73] J. B. Curtis, Z. M. Raines, A. A. Allocca, M. Hafezi, and V. M. Galitski, Phys. Rev. Lett. **122**, 167002 (2019).

[74] G. Mazza and A. Georges, Phys. Rev. Lett. **122**, 017401 (2019).

[75] E. Colella, S. Ostermann, W. Niedenzu, F. Mivehvar, and H. Ritsch, New J. Phys. **21**, 043019 (2019).

[76] S. Uchino, M. Ueda, and J.-P. Brantut, Phys. Rev. A **98**, 063619 (2018).

[77] C. J. Pethick and H. Smith, *Bose-Einstein Condensation in Dilute Gases* (Cambridge University Press, Cambridge, 2001).

[78] M. R. Matthews, D. S. Hall, D. S. Jin, J. R. Ensher, C. E. Wieman, E. A. Cornell, F. Dalfovo, C. Minniti, and S. Stringari, Phys. Rev. Lett. **81**, 243 (1998).

[79] T. Zibold, E. Nicklas, C. Gross, and M. K. Oberthaler, Phys. Rev. Lett. **105**, 204101 (2010).

[80] E. Nicklas, H. Strobel, T. Zibold, C. Gross, B. A. Malomed, P. G. Kevrekidis, and M. K. Oberthaler, Phys. Rev. Lett. **107**, 193001 (2011).

[81] P. B. Blakie, R. J. Ballagh, and C. W. Gardiner, J. Opt. B Quantum Semiclassical Opt. **1**, 378 (1999).

[82] C. P. Search and P. R. Berman, Phys. Rev. A **63**, 043612 (2001).

[83] P. Tommasini, E. J. V. de Passos, A. F. R. de Toledo Piza, M. S. Hussein, and E. Timmermans, Phys. Rev. A **67**, 023606 (2003).

[84] C. Lee, W. Hai, L. Shi, and K. Gao, Phys. Rev. A **69**, 033611 (2004).

[85] I. M. Merhasin, B. A. Malomed, and R. Driben, J. Phys. B: At., Mol. Opt. Phys. **38**, 877 (2005).

[86] M. Abad and A. Recati, Eur. Phys. J. D **67**, (2013).

[87] S. Butera, P. Öhberg, and I. Carusotto, Phys. Rev. A **96**, 013611 (2017).

[88] Z. Chen and B. A. Malomed, Phys. Rev. E **95**, 032217 (2017).

[89] G. Shchedrin, D. Jaschke, and L. D. Carr, Phys. Rev. A **97**, 043601 (2018).

[90] U. Bornheimer, I. Vasić, and W. Hofstetter, Phys. Rev. A **96**, 063623 (2017).

[91] I. Morera, A. Polls, and B. Juliá-Díaz, Sci. Rep. **9**, 9424 (2019).

[92] B. V. Chirikov, Phys. Rep. **52**, 263 (1979).

[93] A. Buchleitner, D. Delande, and J. Zakrzewski, Phys. Rep. **368**, 409 (2002).

[94] M. Hiller, H. Venzl, T. Zech, B. Oleś, F. Mintert, and A. Buchleitner, J. Phys. B: At., Mol. Opt. Phys. **45**, 095301 (2012).

[95] J. Schachenmayer, D. M. Weld, H. Miyake, G. A. Siviloglou, W. Ketterle, and A. J. Daley, Phys. Rev. A **92**, 041602(R) (2015).

[96] Y. Kuno, I. Ichinose, and Y. Takahashi, Sci. Rep. **8**, 10699 (2018).

[97] D. Jaksch and P. Zoller, New J. Phys. **5**, 56 (2003).

[98] S. Al-Assam, S. R. Clark, C. J. Foot, and D. Jaksch, Phys. Rev. B **84**, 205108 (2011).

[99] F. Mezzacapo, N. Schuch, M. Boninsegni, and J. I. Cirac, New J. Phys. **11**, 083026 (2009).

[100] S. de Léséleuc, V. Lienhard, P. Scholl, D. Barredo, S. Weber, N. Lang, H. P. Büchler, T. Lahaye, and A. Browaeys, Science **365**, 775 (2019).

[101] M. Aidelsburger, M. Atala, M. Lohse, J. T. Barreiro, B. Paredes, and I. Bloch, Phys. Rev. Lett. **111**, 185301 (2013).

[102] E. Urban, T. A. Johnson, T. Henage, L. Isenhower, D. Yavuz, T. Walker, and M. Saffman, Nat. Phys. **5**, 110 (2009).

[103] M. A. Cazalilla, Phys. Rev. A **67**, 053606 (2003).